UCRL-ID-139092

Pyrochlore-Rich Titanate Ceramics for the Immobilization of Plutonium: Redox Effects on Phase Equilibria in Cerium- and Thorium-Substituted Analogs

F. J. Ryerson, B. Ebbinghaus

May 25, 2000

U.S. Department of Energy

Lawrence
Livermore
National
Laboratory

DISCLAIMER

This work was performed under the auspices of the U. S. Department of Energy by the University of California, Lawrence Livermore National Laboratory under Contract No. W-7405-Eng-48.

Pyrochlore-rich titanate ceramics for the immobilization of plutonium: Redox effects on phase equilibria in cerium- and thorium- substituted analogs

by

F.J. Ryerson[1] and Bartley Ebbinghaus[2]

1. Earth and Environmental Sciences
Lawrence Livermore National Laboratory
Livermore, CA 94550

2. Chemistry and Material Sciences
Lawrence Livermore National Laboratory
Livermore, CA 94550

UCRL-ID-139092

Abstract. Three compositions representing plutonium-free analogs of a proposed Ca-Ti-Gd-Hf-U-Pu oxide ceramic for the immobilization of plutonium were equilibrated at 1 atm, 1350°C over a range of oxygen fugacities between air and that equivalent to the iron-wüstite buffer. The cerium analog replaces Pu on a mole-per-mole basic with Ce; the thorium analog replaces Pu with Th. A third material has 10 wt% Al_2O_3 added to the cerium analog to encourage the formation of a Hf-analog of, $CaHfTi_2O_7$, zirconolite, which is referred to as hafnolite. The predominant phase produced in each formulation under all conditions is pyrochlore, $A_2T_2O_7$, where the T site is filled by Ti, and Ca, the lanthanides, Hf, U and Pu are accommodated on the A-site. Other lanthanide and uranium-bearing phases encountered include brannerite (UTi_2O_6), hafnolite ($CaHfTi_2O_7$), perovskite ($CaTiO_3$) and a calcium-lanthanide aluminotitanate with nominal stoichiometry $(Ca,Ln)Ti_2Al_9O_{19}$, where Ln is a lanthanide. The phase compositions show progressive shifts with decreasing oxygen fugacity. All of the phases observed have previously been identified in titanate-based high-level radioactive waste ceramics and demonstrate the flexibility of these ceramics to variations in processing parameters.. The main variation is an increase in the uranium concentrations of pyrochlore and brannerite which must be accommodated by variations in modal abundance. Pyrochlore compositions are consistent with existing spectroscopic data suggesting that uranium is predominantly pentavalent in samples synthesized in air. A simple model based on ideal stoichiometry suggests the $U^{+4}/\Sigma U$ varies linearly with log fO_2 and that all of the uranium is quadravalent at the iron-wüstite buffer.

1. Introduction

The Plutonium Immobilization Program has developed a ceramic form suitable for immobilizing surplus plutonium the ceramic is formed by a relatively simple cold press and sinter process The composition and mineralogy of the form is determined by the phase equilibria (Ebbinghaus *et al.* 1999) and is a function of potential processing conditions. The partitioning of the various wastestream components (plutonium, impurity elements and additives) among the crystalline constituents of that phase assemblage may also vary with form composition and processing conditions. Hence, an understanding of the relevant phase equilibria and partitioning relationships as a function of composition and processing conditions is necessary to insure the chemical durability and criticality safety of the resultant wasteform. Chemical durability is most strongly influenced by the mineralogy of the wasteform - are the appropriate phases formed under

a given set of processing conditions, while criticality safety is more strongly influenced by the chemical partitioning - what is the ratio of neutron emittors to absorbers in the constituent phases.

The baseline formulation (Table 1) is designed to produce a pyrochlore ($A_2T_2O_7$)-brannerite (AT_2O_6)-rutile (TO_2) assemblage (Ebbinghaus *et al.* 1999). The T-site in each of these minerals is occupied primarily by titanium. Uranium can also be present in the plutonium feed materials, and is added to the formulation to stabilize pyrochlore. The formulation also contains hafnium, gadolinium and uranium to act as both neutron absorbers in the wasteform itself, or in possible dissolution products (Ebbinghaus et al, 1999). Plutonium, uranium, hafnium and the lanthanides are incorporated in both pyrochlore and brannerite and predominately occupy the A site, which in pyrochlore can also contain a substantial amount of calcium. The formulation contains at least three elements that are commonly found in more than one oxidation state: Pu (+3, +4), U(+4, +5, +6) and Ti (+3, +4, Figure 1). As these are major constituents of the wasteform, variation in the oxygen fugacity during processing is expected to effect the nature of the resulting phase assemblage. Here we present phase equilibria obtained for cerium and thorium-substituted analogs of the baseline formulation (Table 1) for oxygen fugacities between the iron-wüstite buffer and air at 1350°C.

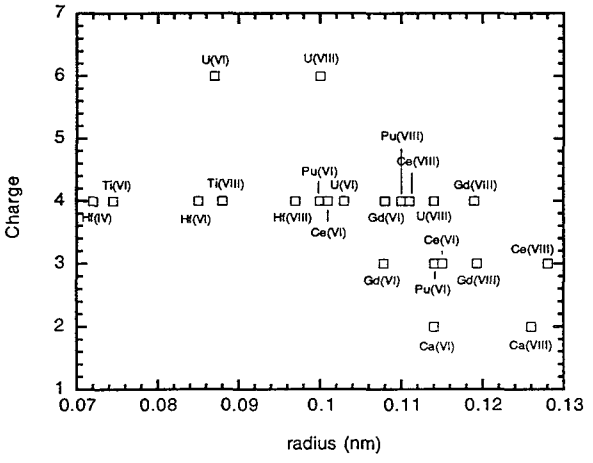

Figure 1. Radius charge relationship for elements relevant to Pu immobilization.

Table 1. Starting compositions (wt%)

	Ce analog	Ce/Al analog	Th analog
Al_2O_3	0.00	10.00	0.00
CaO	10.48	9.32	9.93
TiO_2	36.90	33.55	35.77
HfO_2	11.20	10.02	10.73
CeO_2	8.23	7.35	0.00
Gd_2O_3	8.33	7.52	7.93
ThO_2	0.00	0.00	12.02
UO_2	23.85	22.23	23.63
Total	100.00	100.00	100.00

The baseline mixtures are formulated under the assumption that either cerium or thorium will replace plutonium in the target phases. Cerium exists as both Ce^{+3} and Ce^{+4} with cationic radii close to that of Pu^{+3} and Pu^{+4} and represents a reasonable analog for plutonium under our processing conditions (Table 1). Thorium exists as a quadravalent cation with an ionic radius close to that of Pu^{+4} (Table 1) and allows us to evaluate the effects of uranium oxidation in the absence of another variable valence cation.

Previous results (*cf.*, Ebbinghaus et al, 1999) demonstrate that addition of aluminum to the baseline formulation stabilizes a hafnium-rich analog of zirconolite (ABT_2O_7, hereafter referred to as "hafnolite") that also incorporates Pu (or its analog element) and U as well as the lanthanides. To evaluate the phase equilibria of hafnolite-bearing assemblages, we have also investigated a composition in which 10 wt% Al_2O_3 was added to the cerium-substituted formulation (Table 1).

2. Starting materials and experimental methods

The goal of this investigation is to assess the effects of temperature and oxygen fugacity on phase equilibria at constant temperature, rather than to evaluate process control parameters on other product characteristics. This allows us to make relatively small batches, 1-2 g, of starting materials from mixtures of hydroxides, nitrates, hydrated-nitrates, carbonates, ammoniates and oxides (Table 2). As many of the starting materials

Table 2. Starting materials

Al_2O_3	$Al(OH)_3$
CaO	$CaCO_3$
TiO_2	TiO_2 (rutile)
HfO_2	HfO_2
CeO_2	$(NH_4)_2Ce(NO_3)_6$
Gd_2O_3	$Gd(NO_3)_3 \cdot 6H_2O$
ThO_2	ThO_2
UO_2	$UO_2(NO_3)_2 \cdot 6H_2O$

were extremely hygroscopic, we determined the useful oxide yield of each reagent by loss on combustion. Starting materials were ground by hand under ethanol in an alumina mortar and pestle. The resulting slurry was dried under a heat lamp producing a paste; due to the hygroscopic nature of the material, a fully dry powder was never obtained at this stage of the preparation procedure. The paste was then transferred to a Pt crucible and calcined in air at 1000°C for at least 3 hours. This calcine was then reground by hand under ethanol in an alumina mortar and pestle

prior to the addition of a polyvinyl alcohol solution to act as a binder. The calcine-polyvinyl alcohol slurry was dried under a heat lamp and then ground dry in an alumina mortar and pestle to obtain a free-flowing powder. Individual samples were hand-pressed in a stainless steel die and piston to produce disks approximately 2 mm thick, with an outside diameter of <5 mm, weighing ~50 mg.

Table 3. Run Conditions and results

1/3	Hf-Ce-U	1350	-0.69	pyr, rut
1/4	Hf-Ce-U	1350	-2.6	pyr, brn, rut
1/5	Hf-Ce-U	1350	-5.05	pyr, rut
1/6	Hf-Ce-U	1350	-5.9	pyr, rut
1/9	Hf-Ce-U	1350	-6.83	pyr, hfn, pv, rut
1/7	Hf-Ce-U	1350	-8.00	pyr, hfn, pv, rut
1/8	Hf-Ce-U	1350	-10.06	pyr, hfn, pv
7/3	Hf-Ce-U + Al_2O_3	1350	-0.69	pyr, brn, hfn, psb
7/4	Hf-Ce-U + Al_2O_3	1350	-2.6	pyr, hfn, brn, rut, CTA
7/5	Hf-Ce-U + Al_2O_3	1350	-5.05	pyr, hfn, brn, rut, CTA
7/6	Hf-Ce-U + Al_2O_3	1350	-5.9	pyr, hfn, rut, CTA
7/9	Hf-Ce-U + Al_2O_3	1350	-6.83	pyr, hfn, pv, CTA
7/7	Hf-Ce-U + Al_2O_3	1350	-8.00	pyr, hfn, pv, CTA
7/8	Hf-Ce-U + Al_2O_3	1350	-10.06	pyr, hfn, pv, CTA
8/3	Hf-Th-U	1350	-0.69	pyr, brn, rut
8/4	Hf-Th-U	1350	-2.6	pyr, brn, rut, hfn
8/5	Hf-Th-U	1350	-5.05	pyr, brn, rut, hfn
8/6	Hf-Th-U	1350	-5.9	pyr, brn, rut, hfn
8/9	Hf-Th-U	1350	-6.83	pyr, brn, rut, hfn
8/7	Hf-Th-U	1350	-8.00	pyr, brn, rut
8/8	Hf-Th-U	1350	-10.06	pyr, brn, rut,hfn

rut=rutile, pyr=pyrochlore, hfn=hafnolite, brn = brannerite,
psb= Al-Ti psuedobrookite, pv=perovskite, CTA=Calcium-lathanide titanoaluminate

A bottom-loading Deltech furnace was used to anneal samples equilibrated in air. Samples were loaded in open Pt crucibles that were then placed on the lower platen of the furnace and hydraulically lifted into the furnace that was already at run temperature. Temperature was monitored using a Pt-Rh thermocouple placed within 5 mm of the sample. Samples reached run conditions within 2-4 minutes after insertion, and run duration was always in excess of 23 hours. Runs were quenched by lowering the platen and removing the crucibles that then cooled in air. The lower oxygen fugacities runs were equilibrated in Deltech furnace equipped with a vertical alumina muffle tube, and oxygen fugacity was controlled using CO-CO_2 gas mixtures. The fO_2 was

monitored with a zirconia sensor cell and temperature was measured using a Pt-Rh thermocouple placed within 2 mm of the sample that was suspended from an alumina rod. The samples were contained in a 5 mm diameter Pt capillary that was partially crimped at both ends allowing continual contact between the sample and the gas mixture. The samples were plunged into the top of the furnace at run conditions and reached final temperature within 5 minutes. Samples were quenched by pulling the alumina rod-sample assembly from the top of the furnace and cooled in air. Run conditions and products are given in Table 3.

3. Sample characterization

The sintered disks were mounted in epoxy and then polished with alumina grits prior to final polishing on a colloidal silica polisher. The polished mounts were then carbon coated for SEM and electron probe analysis. Compositional analysis was performed on a JEOL-733 electron probe using wavelength dispersive analysis. The probe was operated at an accelerating voltage of 15 KV with a beam current (measured in a Faraday cup embedded in the sample stage) of 30-100 na. X-ray intensities were reduced to oxides using the ZAF method as revised by Armstrong et al. (1995). Two notable x-ray interferences were observed. The $Ce_{L\beta 1}$ line interferes with the Gd $_{L\alpha 1}$ requiring the use of the Gd $_{L\beta 1}$ line. In the Th-bearing samples, the $Th_{M\beta 1}$ interferes with the $U_{M\alpha 1\text{-}1}$ requiring use of the $U_{M\beta 1}$ line.

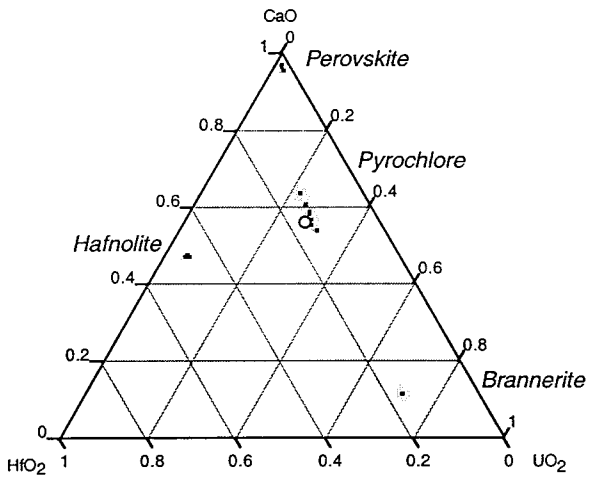

Figure 2. $CaO\text{-}HfO_2\text{-}UO_2$ diagram showing the compositions of perovskite, pyrochlore, hafnolite and brannerites from Ce-analog materials sintered at 1350°C. Pyrochlores become richer in uranium with decreasing fO_2. The bulk composition is given by the open circle.

4. Results

4.1 Cerium-substituted analog

The phase assemblages for these experiments are given in Table 3 and the compositions of the individual phases in Table 4. Runs were performed in air, and at 6 other oxygen fugacities. The assemblage found in the higher fO_2 runs (-log fO_2 <5.9) is pyrochlore, rutile, ± brannerite. As fO_2 decreases, brannerite is not observed, and is replaced by hafnolite and perovskite.

Table 4. Electron microprobe analyses of phases in the Ce-analog at 1350°C

	1-3 $\log fO_2$ = -0.69				1-4 $\log fO_2$ = -2.6						1-5 $\log fO_2$ = -5.05			
	Pyrochlore	9	Rutile	3	Pyrochlore	6	Brannerite	5	Rutile	4	Pyrochlore	6	Rutile	4
	wt%	std dev	wt%	std dev	wt%	std dev	wt%	std dev	wt%	std dev	wt%	std dev	wt%	std dev
Al_2O_3	0.16	0.01	0.69	0.03	0.27	0.01	0.43	0.01	0.53	0.02	0.12	0.01	0.43	0.01
CaO	12.53	1.17	0.01	0.01	12.08	0.13	1.17	0.25	0.15	0.06	10.92	0.13	0.15	0.03
TiO_2	33.86	1.27	78.30	0.95	33.99	0.29	39.81	0.39	78.68	0.27	35.33	0.19	81.81	0.53
Ce_2O_3	8.87	0.60	0.04	0.02	8.89	0.23	8.79	0.34	0.07	0.02	8.53	0.16	0.13	0.06
Gd_2O_3	9.30	0.95	0.00	0.00	9.62	0.29	6.34	0.27	0.16	0.05	8.95	0.21	0.14	0.05
HfO_2	10.23	0.47	18.50	0.85	10.36	0.17	6.24	0.41	17.44	0.22	9.98	0.21	15.48	0.26
UO_2	20.95	1.91	2.39	0.20	23.72	0.31	34.69	0.80	2.45	0.09	24.08	0.24	1.62	0.05
Total	95.89	-	99.93	-	98.94	-	97.48	-	99.47	0.33	97.91	-	99.76	0.43
Al	0.015	0.002	0.012	0.001	0.024	0.001	0.033	0.001	0.010	0.000	0.011	0.001	0.007	0.000
Ca	1.012	0.041	0.000	0.000	0.968	0.013	0.081	0.017	0.002	0.001	0.888	0.009	0.002	0.001
Ti	1.925	0.059	0.898	0.006	1.911	0.006	1.930	0.019	0.903	0.002	2.016	0.012	0.918	0.001
Ce	0.245	0.006	0.000	0.000	0.243	0.005	0.208	0.008	0.000	0.000	0.237	0.005	0.001	0.000
Gd	0.232	0.012	0.000	0.000	0.238	0.006	0.136	0.006	0.001	0.000	0.225	0.005	0.001	0.000
Hf	0.221	0.005	0.081	0.004	0.221	0.004	0.115	0.008	0.076	0.001	0.216	0.004	0.066	0.001
U	0.351	0.018	0.008	0.001	0.395	0.004	0.498	0.010	0.008	0.000	0.407	0.003	0.005	0.000
Catatoms	4.000	0.000	1.000	0.000	4.000	0.000	3.000	0.000	1.000	0.000	4.000	0.000	1.000	0.000
Oxygen	6.743	0.046	1.994	0.000	6.779	-	5.731	-	1.992	-	6.875	-	1.993	-
$Ce^{+4}/\Sigma Ce$	0.33		0.00		0.26		0.26		0.00		0.18		0.00	
Ca	0.000		0.000		0.000		0.000		0.000		0.000		0.000	
Gd	0.000		0.000		0.000		0.000		0.000		0.000		0.000	
Ce^{+3}	0.000		0.000		0.000		0.000		0.000		0.000		0.000	
Ce^{+4}	0.000		0.000		0.000		0.000		0.000		0.000		0.000	
Sum	0.000		0.000		0.000		0.000		0.000		0.000		0.000	
Charge	0.000		0.000		0.000		0.000		0.000		0.000		0.000	
Ca	1.012		0.000		0.968		0.081		0.000		0.888		0.000	
Al	0.000		0.000		0.000		0.000		0.000		0.011		0.000	
Ce^{+3}	0.164		0.000		0.179		0.153		0.000		0.195		0.000	
Ce^{+4}	0.081		0.000		0.064		0.055		0.000		0.042		0.000	
Gd	0.232		0.000		0.238		0.136		0.000		0.225		0.000	
Hf	0.160		0.000		0.156		0.078		0.000		0.216		0.000	
U	0.351		0.000		0.395		0.498		0.000		0.407		0.000	
Sum	2.000		0.000		2.000		1.000		0.000		1.984		0.000	
Charge	6.015		0.000		6.024		4.033		0.000		5.969		0.000	
Ti	1.925		0.898		1.911		1.930		0.903		2.016		0.918	
Hf	0.061		0.081		0.065		0.037		0.076		0.000		0.066	
Al	0.015		0.012		0.024		0.033		0.010		0.000		0.007	
Sum	2.000		0.992		2.000		2.000		0.988		2.016		0.991	
Charge	7.985		3.954		7.976		7.967		3.943		8.064		3.956	
Total	4.000		0.992		4.000		3.000		0.988		4.000		0.991	
UO_2	2.617		2.000		2.478		2.486		2.000		2.296		2.000	
Total	4.000		0.992		4.000		3.000		0.988		4.000		0.991	
Model Oxygens	7.000		1.977		7.000		6.000		1.971		7.000		1.978	

Table 4 (cont.). Electron microprobe analyses of phases in the Ce-analog at 1350°C

	1-6 $\log fO_2$ = -5.9				1-7 $\log fO_2$ = -8.00								1-8 $\log fO_2$ = -10.06					
	Pyrochlore	6	Rutile	4	Pyrochlore	6	Hafnolite	6	Perovskite	5	Rutile	4	Pyrochlore	6	Hafnolite	6	Perovskite	6
	wt%	std dev	wt%	std dev	wt%	std dev	wt%	std dev	wt%	std dev	wt%	std dev	wt%	std dev	wt%	std dev	wt%	std dev
Al_2O_3	0.12	0.01	0.43	0.01	0.10	0.01	2.21	0.04	0.73	0.03	0.32	0.01	0.10	0.01	1.77	0.03	0.56	0.05
CaO	10.85	0.08	0.14	0.03	10.17	0.05	9.93	0.12	20.35	0.12	0.15	0.06	9.65	0.08	9.48	0.06	20.03	0.21
TiO_2	35.78	0.19	83.62	0.11	35.83	0.11	37.03	0.58	48.43	0.25	83.67	0.43	35.69	0.25	38.30	0.20	47.84	0.31
Ce_2O_3	8.41	0.24	0.06	0.05	7.48	0.23	3.19	0.11	23.68	0.45	0.01	0.03	6.93	0.19	3.19	0.13	23.05	1.22
Gd_2O_3	8.82	0.20	0.14	0.04	9.18	0.19	5.34	0.20	4.98	0.13	0.01	0.01	9.16	0.15	5.89	0.23	5.25	0.36
HfO_2	9.94	0.18	14.08	0.27	10.64	0.21	37.56	1.00	1.23	0.08	14.74	0.22	10.12	0.20	35.45	0.83	1.26	0.32
UO_2	24.11	0.39	1.22	0.06	25.37	0.08	4.71	0.10	1.64	0.07	0.69	0.04	26.40	0.54	5.43	0.20	2.34	0.78
Total	98.03	-	99.68	0.26	98.76	-	99.97	-	101.02	-	99.59	0.20	98.05	-	99.51	-	100.32	-
Al	0.011	0.001	0.007	0.000	0.009	0.001	0.187	0.002	0.024	0.001	0.006	0.000	0.009	0.001	0.151	0.002	0.019	0.002
Ca	0.879	0.006	0.002	0.000	0.831	0.004	0.762	0.005	0.622	0.002	0.002	0.001	0.801	0.006	0.732	0.004	0.621	0.006
Ti	2.035	0.007	0.926	0.002	2.056	0.006	1.996	0.020	1.039	0.006	0.928	0.002	2.080	0.010	2.076	0.013	1.040	0.004
Ce	0.233	0.006	0.000	0.000	0.209	0.007	0.084	0.003	0.247	0.004	0.000	0.000	0.197	0.006	0.084	0.003	0.244	0.013
Gd	0.221	0.005	0.001	0.000	0.232	0.005	0.127	0.005	0.047	0.001	0.000	0.000	0.235	0.004	0.141	0.006	0.050	0.004
Hf	0.215	0.004	0.059	0.001	0.232	0.004	0.769	0.025	0.010	0.001	0.062	0.001	0.224	0.004	0.729	0.016	0.010	0.003
U	0.406	0.006	0.004	0.000	0.431	0.001	0.075	0.001	0.010	0.000	0.002	0.000	0.455	0.010	0.087	0.003	0.015	0.005
Catatoms	4.000	0.000	1.000	0.000	4.000	0.000	4.000	0.000	2.000	0.000	1.000	0.000	4.000	0.000	4.000	0.000	2.000	0.000
Oxygen	6.888	-	1.994	-	6.943	-	7.039	-	3.219	-	1.995	-	6.979	-	7.080	-	3.223	-
$Ce^{+4}/\Sigma Ce$	0.15		0.00		0.07		0.07		0.07		0.00		0.00		0.00		0.00	
Ca	0.000		0.000		0.000		0.762		0.000		0.000		0.000		0.732		0.000	
Gd	0.000		0.000		0.000		0.127		0.000		0.000		0.000		0.141		0.000	
Ce^{+3}	0.000		0.000		0.000		0.078		0.000		0.000		0.000		0.084		0.000	
Ce^{+4}	0.000		0.000		0.000		0.006		0.000		0.000		0.000		0.000		0.000	
Sum	0.000		0.000		0.000		0.967		0.000		0.000		0.000		0.957		0.000	
Charge	0.000		0.000		0.000		2.162		0.000		0.000		0.000		2.139		0.000	
Ca	0.879		0.000		0.831		0.000		0.622		0.000		0.801		0.000		0.621	
Al	0.011		0.000		0.009		0.183		0.024		0.000		0.009		0.151		0.019	
Ce^{+3}	0.199		0.000		0.194		0.006		0.229		0.000		0.197		0.000		0.244	
Ce^{+4}	0.034		0.000		0.015		0.000		0.018		0.000		0.000		0.000		0.000	
Gd	0.221		0.000		0.232		0.000		0.047		0.000		0.235		0.000		0.050	
Hf	0.215		0.000		0.232		0.769		0.010		0.000		0.224		0.729		0.010	
U	0.406		0.000		0.431		0.075		0.010		0.000		0.455		0.087		0.015	
Sum	1.965		0.000		1.944		1.033		0.961		0.000		1.920		0.967		0.960	
Charge	5.893		0.000		5.806		3.944		2.300		0.000		5.708		3.717		2.284	
Ti	2.035		0.926		2.056		1.996		1.039		0.928		2.080		2.076		1.040	
Hf	0.000		0.059		0.000		0.000		0.000		0.062		0.000		0.000		0.000	
Al	0.000		0.007		0.000		0.004		0.000		0.006		0.000		0.000		0.000	
Sum	2.035		0.993		2.056		2.000		1.039		0.995		2.080		2.076		1.040	
Charge	8.140		3.964		8.223		7.996		4.156		3.976		8.318		8.304		4.162	
Total	4.000		0.993		4.000		4.000		2.000		0.995		4.000		4.000		2.000	
UO_x	2.275		2.000		2.147		2.000		2.000		2.000		2.076		2.000		2.000	
Model Oxygens	7.000		1.982		7.000		7.051		3.228		1.988		7.000		7.080		3.223	

Table 4 (cont.). Electron microprobe analyses of phases in the Ce-analog at 1350°C

	1-9 $\log fO_2$ = -6.83							
	Pyrochlore	6	Hafnolite	6	Perovskite	6	Rutile	5
	wt%	std dev	wt%	std dev	wt%	std dev	wt%	std dev
Al_2O_3	0.12	0.03	2.40	0.09	0.77	0.04	0.36	0.01
CaO	10.36	0.09	9.92	0.13	20.51	0.96	0.12	0.04
TiO_2	35.56	0.18	36.42	0.22	48.35	0.43	83.49	0.74
Ce_2O_3	7.99	0.13	3.30	0.23	22.74	1.69	0.11	0.03
Gd_2O_3	8.82	0.15	5.46	0.11	5.23	0.43	0.01	0.02
HfO_2	10.24	0.23	36.47	0.63	0.97	0.09	14.25	0.22
UO_2	24.73	0.24	4.94	0.13	1.47	0.04	0.94	0.05
Total	97.81	-	98.89	-	100.04	-	99.28	0.87
Al	0.011	0.003	0.204	0.007	0.026	0.002	0.006	0.000
Ca	0.850	0.006	0.768	0.009	0.628	0.023	0.002	0.001
Ti	2.047	0.009	1.979	0.009	1.040	0.006	0.928	0.001
Ce	0.224	0.004	0.087	0.006	0.238	0.020	0.001	0.000
Gd	0.224	0.003	0.131	0.002	0.050	0.004	0.000	0.000
Hf	0.224	0.005	0.752	0.014	0.008	0.001	0.060	0.001
U	0.421	0.004	0.079	0.002	0.009	0.000	0.003	0.000
Catatoms	4.000	0.000	4.000	0.000	2.000	0.000	1.000	0.000
Oxygen	6.921	-	7.021	-	3.215	-	1.995	-
$Ce^{+4}/\Sigma Ce$	0.11		0.11		0.11		0.00	
Ca	0.000		0.768		0.000		0.000	
Gd	0.000		0.131		0.000		0.000	
Ce^{+3}	0.000		0.077		0.000		0.000	
Ce^{+4}	0.000		0.010		0.000		0.000	
Sum	0.000		0.975		0.000		0.000	
Charge	0.000		2.198		0.000		0.000	
Ca	0.850		0.000		0.628		0.000	
Al	0.011		0.183		0.026		0.000	
Ce^{+3}	0.198		0.077		0.211		0.000	
Ce^{+4}	0.025		0.010		0.027		0.000	
Gd	0.224		0.000		0.050		0.000	
Hf	0.224		0.752		0.008		0.000	
U	0.421		0.079		0.009		0.000	
Sum	1.953		1.102		0.960		0.000	
Charge	5.845		4.147		2.295		0.000	
Ti	2.047		1.979		1.040		0.928	
Hf	0.000		0.000		0.000		0.060	
Al	0.000		0.021		0.000		0.006	
Sum	2.047		2.000		1.040		0.994	
Charge	8.187		7.979		4.162		3.971	
UO_x	2.196		2.000		2.000		2.000	
Total	4.000		4.077		2.000		0.994	
Model Oxygens	7.000		7.162		3.228		1.986	

LEFT INTENTIONALLY BLANK

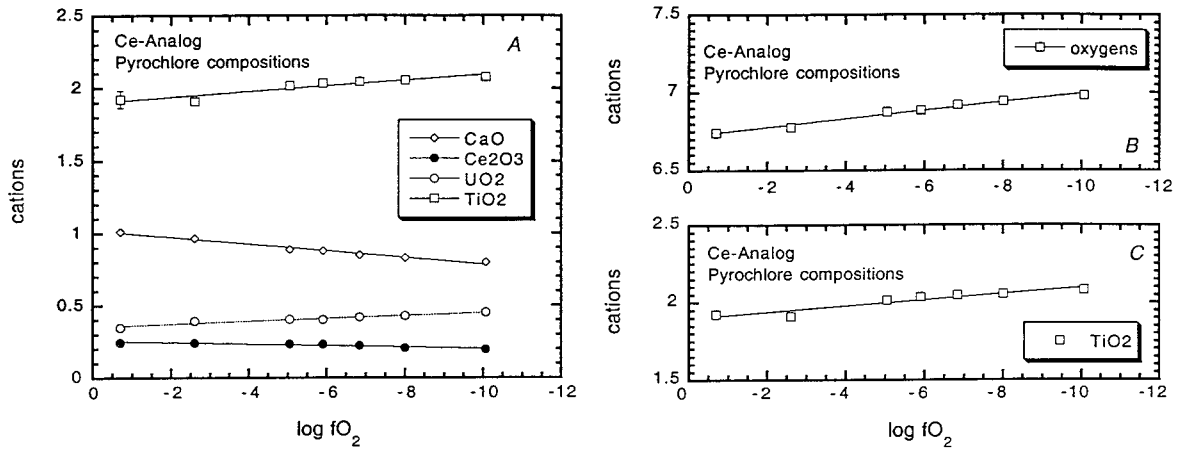

Figure 3. (A) Cation concentrations (normalized to 4 cations) in pyrochlore as a function of oxygen fugacity for the Ce-analog mixture. (B) Oxygen concentration assuming trivalent Ce and quadravalent U. (C) Ti concentration (normalized to 4 cations) in pyrochlore as a function of oxygen fugacity for the Ce-analog mixture.

The average phase compositions from the 1350_C runs (mole%) are plotted onto the CaO-HfO2-UO2 ternary in Figure 2. The most striking feature of these data is the linear trend, parallel to the CaO-UO_2 axis, formed by the pyrochlore compositions, indicating an inverse correlation between CaO and UO_2 concentrations at close-to-constant HfO_2. The run conducted in air anchors the CaO-rich end of this array and UO_2 is exchanged for CaO as fO_2 is decreased. Brannerite plots close to the UO_2 apex, and although the number of brannerite analyses is small they also appear to show a dependence on fO_2 and UO_2 decreasing at constant Ca/Hf with increasing fO_2 (Figure 2). Hafnolite plots along the CaO-HfO_2 join, and perovskite at the CaO apex; neither phase displays a great deal of chemical variation on this plot. Also plotted is the starting composition which falls just to the HfO_2 side of the pyrochlore array. The proximity of the bulk and pyrochlore compositions is consistent with the modal predominance of this phase. On a weight percent basis, the plutonium analog-element, cerium, is equally partitioned between brannerite

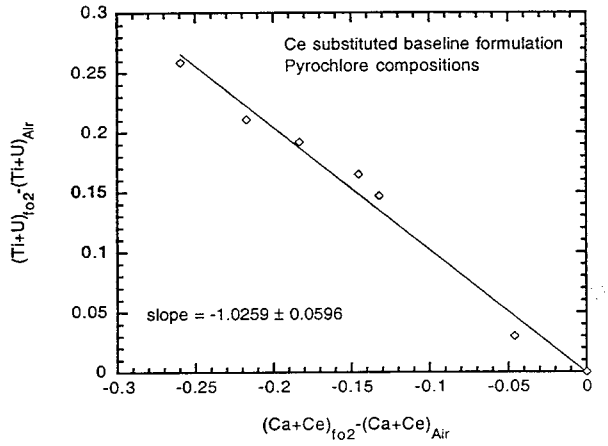

Figure 4. The variation in Ti + U in pyrochlores sintered under reducing conditions relative to those sintered in air as a function of the change in Ca + Ce sintered under reducing conditions relative to those sintered in air. The slope of unity indicates the coupling of these cations, and perhaps the destabilization of cerium-bearing pyrochlores at lower oxygen fugacities.

and pyrochlore, with pyrochlore slightly enriched in Gd_2O_3 and HfO_2 relative to brannerite (Table

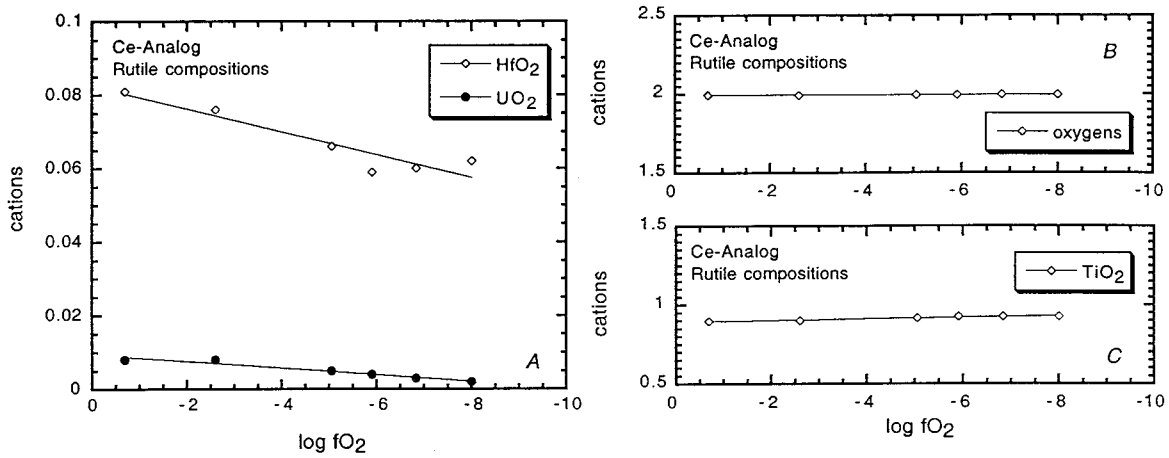

Figure 5. (A) Cation concentrations (normalized to 4 cations) in pyrochlores as a function of oxygen fugacity for the Ce-analog mixture. (B) Oxygen concentration assuming trivalent Ce and quadravalent U. (C) Ti concentration (normalized to 4 cations) in rutile as a function of oxygen fugacity for the Ce-analog mixture.

4). Brannerite contains approximately 50% more UO_2 than the coexisting pyrochlore. Hafnolite is extremely enriched in HfO_2 with respect to the other phases, and also contains 3-6 wt% of Ce_2O_3, Gd_2O_3 and UO_2. Perovskite contains as much as 23 wt% Ce_2O_3; in Pu-bearing materials, perovskite is, therefore, expected to incorporate Pu.

The stoichiometry of the pyrochlores is consistent with a T-site that is essentially fully occupied by

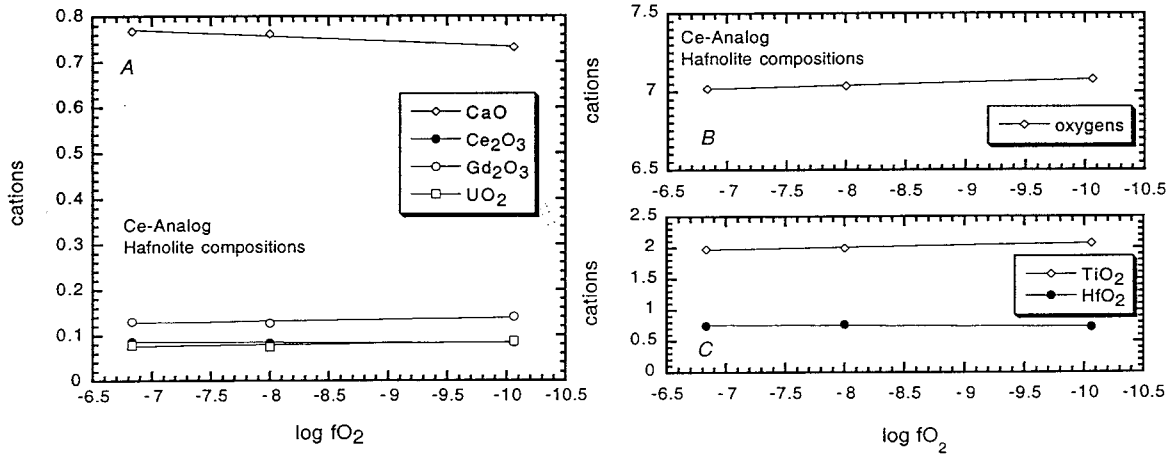

Figure 6. Cation concentrations (normalized to 1 cation) in perovskites as a function of oxygen fugacity for the Ce-analog mixture.

titanium – 2 Ti cations per 4 total cations (Table 4). The Ti concentration of brannerite is also close

to 2 Ti per 4 total cations indicating that the T-site in brannerites is essentially fully occupied by

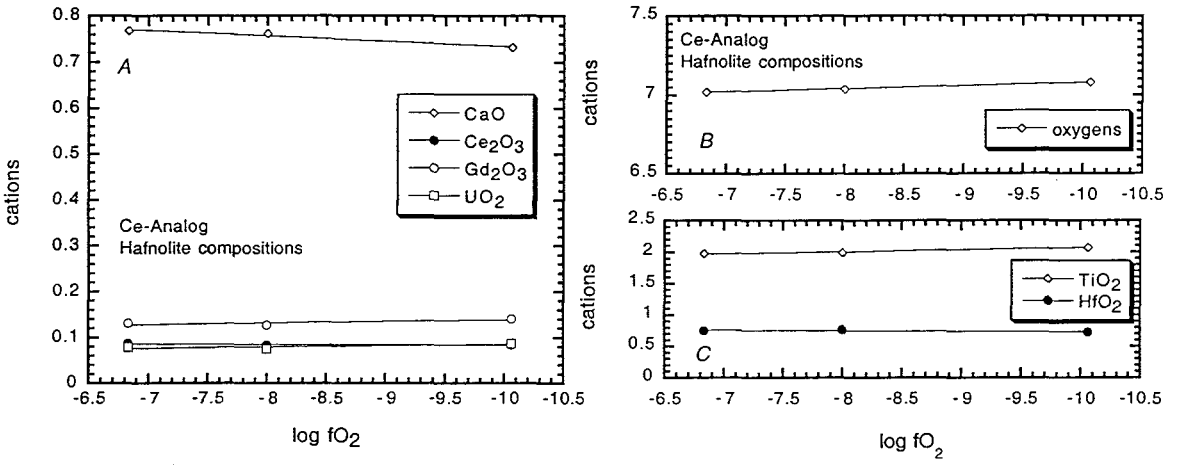

Figure 7. (A) Cation concentrations (normalized to 4 cations) in hafnolite as a function of oxygen fugacity for the Ce-analog mixture. (B) Oxygen concentration assuming trivalent Ce and quadravalent U. (C) Ti and Hf concentration (normalized to 4 cations) in pyrochlores as a function of oxygen fugacity for the Ce-analog mixture.

titanium. This is also true of the hafnolites which typically have ~2 Ti cations per 4 total cations. However, the Ca content of hafnolite is always less than one indicating that the A-site in this phase is partially occupied by other elements.

The variation in pyrochlore chemistry is better displayed by plotting the cation concentrations (normalized to 4 cations) *vs* fO_2 (Figure 3). The cation concentrations and the model oxygen stoichiometry vary smoothly with fO_2, displaying no distinct discontinuity at the "hafnolite-in" boundary. The concentrations of Hf and Gd do not vary with respect to log fO_2. The concentrations of Ti and U in pyrochlore all increase with decreasing fO_2. To compensate for the increases in the concentrations of Ti and U, the number of both Ca and Ce cations per 4 cations decreases as a function of fO_2. In fact, relative to their concentrations in air, the changes in Ca+Ce and Ti+U with decreasing fO_2 are, within error, exactly compensated (Figure 4).

A model oxygen stoichiometry (total oxygen atoms per 4 cations) can also be calculated by assuming that uranium is present as U^{+4} and cerium as Ce^{+3}. The number of oxygen atoms normalized to 4 cations increases from ~6.74 for samples sintered in air to close to the ideal stoichiometry of 7 oxygens normalized to 4 cations for samples sintered at -log fO_2 ~10 (Figure 3b). This trend suggests that, for experiments equilibrated at higher fO_2 greater than -log fO_2 ~ 10, either uranium or cerium may be present in a higher oxidation site than assumed in the model.

The composition of rutile also shows a systematic change with fO_2 (Figure 5 a,b). The

concentrations of U and Hf both decrease as the processing conditions become more reducing. The model oxygen stoichiometry is relatively constant over this range, so it is difficult to determine whether the variation in rutile chemistry is a function of changes in oxidation state within the rutile itself, or reflective of variations in the partition coefficients with fO_2.

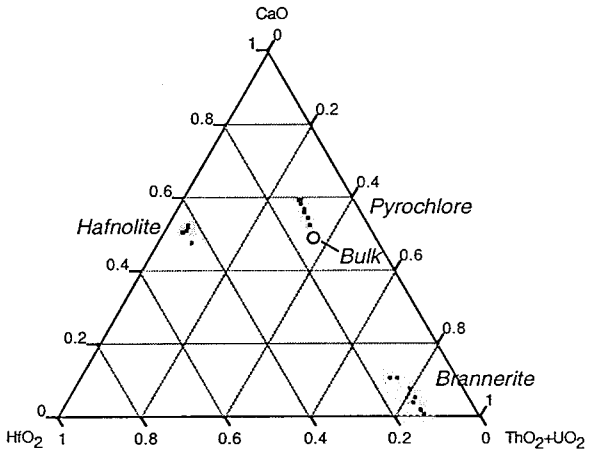

Figure 8. CaO-HfO_2-(UO_2+ThO_2) from Th-analog materials sintered at 1350°C. Pyrochlore and brannerite becomes richer in uranium with decreasing fO_2. The bulk composition is given by the open circle.

The major mineralogical change that takes place with decreased fO_2 is the appearance of perovskite and hafnolite. Perovskite is enriched in calcium and the lanthanides, and the release of these elements from pyrochlore likely stabilizes this phase. The composition of perovskite shows little change with fO_2 (Figures 2 and 6). The number of oxygens based on 2 cations (assuming U^{+4} and Ce^{+3}) is always greater than the 3 oxygens equivalent to the ideal stoichiometry. This is indicative of cation vacancies in the perovskite structure. Hafnolite strongly concentrates and is stabilized by the presence of hafnium. Its appearance at lower fO_2s may be coupled with the decreasing concentrations of Hf in rutile, and the eventual disappearance of rutile in the lowest fO_2 experiments. Like pyrochlore, the Ca content of hafnolite decreases somewhat with decreasing fO_2 and appears to be coupled to increased U (Figure 7).

4.2 Thorium-substituted analog

The Th-substituted baseline composition is formulated as a mole-per-mole replacement of Ce by Th (Table 1) and allows us to evaluate the phase equilibria in an analog system in which uranium is the only element likely to occur in multiple valence states under the T-fO_2 range of these experiments. The major difference in the mineralogy between the Th- and Ce-substituted analogs is the ubiquity of brannerite and absence of perovskite in the Th-substituted formulation (Table 3). At 1350°C in air, the observed assemblage is pyrochlore-brannerite-rutile. Under conditions more reducing than air the assemblage is pyrochlore-brannerite-rutile±hafnolite. The compositions of coexisting phases are given in Table 5 and plotted on the CaO-HfO_2-(UO_2+ThO_2) (Figure 8). The simplest interpretation of these results is that the addition of Th stabilizes brannerite, and by extension, if Th^{+4} is an analog for U^{+4}, then brannerite should be stabilized under reducing conditions in Th-free formulations. The absence of perovskite can be explained by the absence of cerium which is strongly concentrated in, and hence, stabilizes perovskite.

The pyrochlore compositions form a linear array parallel to the CaO-(ThO_2+UO_2) axis and, like the pyrochlores in the Ce-substituted assemblages, become more (ThO_2+UO_2)-rich with decreasing fO_2 (Figure 8). Brannerite also forms and array parallel to the CaO-(ThO_2+UO_2) axis and, like the pyrochlores becomes richer in UO_2 as fO_2 decreases. The hafnolites form a relatively tight cluster, plotting in a position similar to those in the Ce-analog experiments.

At the higher fO_2s UO_2 is equally distributed between brannerite and pyrochlore with both phases containing ~20 wt% UO_2. Hafnolite is much poorer than either brannerite or pyrochlore in both UO_2 (typically ~4 wt%) and ThO_2 (1 wt%). Hafnolite does concentrate HfO_2 containing roughly 4 and 5 times that in pyrochlore and brannerite, respectively.

In these pyrochlores, the Ca cation concentration per 4 cations is actually greater than one, and there is sufficient titanium to fill the T-site (Table 5). The T-site in brannerite can also be filled with titanium with ~2 Ti per 4 cations. Unlike the Ce-analog samples, the A-site in the Th-analog

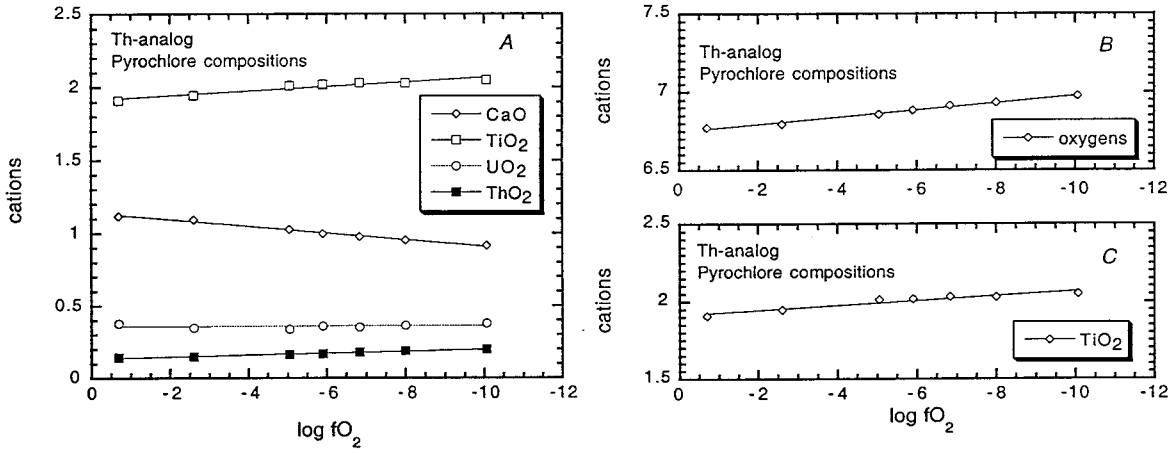

Figure 9. (A) Cation concentrations (normalized to 4 cations) in pyrochlore as a function of oxygen fugacity for the Th-analog mixture. (B) Oxygen concentration assuming trivalent Ce and quadravalent U. (C) Ti concentration (normalized to 4 cations) in pyrochlores as a function of oxygen fugacity for the Th-analog mixture.

hafnolites is essentially filled with calcium; 1 Ca per 4 total cations. This may reflect the reduced lanthanide budget, allowing Gd to be totally accommodated on the B-site in the Th-analog hafnolites.

Table 5. Electron probe results and structural formulae for Th-analog experiments

	8-3 $\log fO_2$=-0.69						8-4 $\log fO_2$=-2.6							
	Pyrochlore	6	Brannerite	6	Rutile	3	Pyrochlore	7	Brannerite	6	Hafnolite	3	Rutile	3
	wt%	std dev	wt%	std dev	wt%	std dev	wt%	std dev	wt%	std dev	wt%	std dev	wt%	std dev
Al_2O_3	0.00	0.00	0.04	0.10	0.30	0.01	0.05	0.02	0.20	0.01	1.29	0.07	0.30	0.15
CaO	14.03	0.05	1.36	0.07	0.08	0.02	13.47	0.21	1.23	0.07	11.57	0.38	0.05	0.01
TiO_2	34.14	0.10	39.60	0.23	79.10	0.77	34.19	0.60	38.53	0.54	36.08	0.93	80.95	0.72
Gd_2O_3	8.85	0.20	5.87	0.16	0.15	0.04	8.72	0.22	5.49	0.39	4.65	0.38	0.00	0.00
HfO_2	10.91	0.16	7.59	0.39	19.15	0.53	11.08	0.18	6.53	1.27	39.45	1.84	16.38	0.22
ThO_2	8.48	0.31	22.14	0.77	0.06	0.03	8.64	0.16	21.60	1.51	1.09	0.01	0.00	0.00
UO_2	23.00	0.29	21.70	0.61	1.44	0.03	20.72	0.50	22.49	0.97	4.32	0.49	1.05	0.09
Total	99.40	-	98.31	-	100.29	-	96.87	-	96.05	-	98.46	-	98.73	-
Al	0.000	0.000	0.003	0.008	0.005	0.000	0.004	0.002	0.016	0.001	0.107	0.003	0.006	0.002
Ca	1.118	0.004	0.097	0.005	0.001	0.000	1.093	0.013	0.098	0.006	0.972	0.012	0.003	0.003
Ti	1.909	0.004	1.974	0.003	0.904	0.003	1.947	0.019	1.964	0.017	1.934	0.017	0.917	0.005
Gd	0.218	0.005	0.129	0.004	0.001	0.000	0.219	0.007	0.123	0.009	0.109	0.005	0.000	0.000
Hf	0.232	0.003	0.144	0.007	0.083	0.003	0.240	0.005	0.126	0.024	0.792	0.039	0.070	0.001
Th	0.143	0.005	0.334	0.012	0.000	0.000	0.149	0.004	0.333	0.024	0.018	0.000	0.000	0.000
U	0.380	0.004	0.320	0.010	0.005	0.000	0.349	0.008	0.339	0.015	0.069	0.005	0.004	0.001
Catatoms	4.000	-	3.000	-	1.000	-	4.000	0.000	3.000	0.000	4.000	0.000	1.000	0.000
oxygen	6.773	-	5.837	-	2.005	-	6.796	-	5.832	-	6.921	-	1.994	-
Ca	0.000		0.000		0.000		0.000		0.000		0.972		0.000	
Gd	0.000		0.000		0.000		0.000		0.000		0.028		0.000	
Th	0.000		0.000		0.000		0.000		0.000		0.000		0.000	
Sum	0.000		0.000		0.000		0.000		0.000		1.000		0.000	
Charge	0.000		0.000		0.000		0.000		0.000		2.028		0.000	
Ca	1.118		0.097		0.000		1.093		0.098		0.000		0.000	
Al	0.000		0.000		0.000		0.000		0.000		0.041		0.000	
Gd	0.218		0.129		0.000		0.219		0.123		0.080		0.000	
Hf	0.140		0.120		0.000		0.190		0.106		0.792		0.000	
Th	0.143		0.334		0.000		0.149		0.333		0.018		0.000	
U	0.380		0.320		0.000		0.349		0.339		0.069		0.000	
Sum	2.000		1.000		0.000		2.000		1.000		1.000		0.000	
Charge	6.000		4.003		0.000		6.004		4.016		4.037		0.000	
Ti	1.909		1.974		0.904		1.947		1.964		1.934		0.917	
Hf	0.091		0.023		0.083		0.049		0.020		0.000		0.070	
Al	0.000		0.003		0.005		0.004		0.016		0.066		0.006	
Sum	2.000		2.000		0.993		2.000		2.000		2.000		0.993	
Charge	8.000		7.997		3.966		7.996		7.984		7.997		3.967	
UO_4	2.596		2.509		2.000		2.586		2.495		3.148		2.000	
Total Cations	4.000		3.000		0.993		4.000		3.000		4.000		0.993	
Model Oxygens	7.000		6.000		1.983		7.000		6.000		7.000		1.983	

Table 5. (cont.) Electron probe results and structural formulae for Th-analog experiments

	8-5 $\log fO_2$=-5.05								8-6 $\log fO_2$=-5.9							
	Pyrochlore	6	Brannerite	5	Hafnolite	4	Rutile	3	Pyrochlore	6	Brannerite	4	Hafnolite	3	Rutile	3
	wt%	std dev	wt%	std dev	wt%	std dev	wt%	std dev	wt%	std dev	wt%	std dev	wt%	std dev	wt%	std dev
Al_2O_3	0.11	0.01	0.26	0.03	1.51	0.02	0.24	0.01	0.07	0.04	0.17	0.02	1.63	0.23	0.15	0.02
CaO	12.62	0.09	0.91	0.17	11.59	0.07	0.14	0.05	12.20	0.21	0.63	0.05	11.29	0.23	0.03	0.04
TiO_2	35.21	0.40	37.22	0.87	36.61	0.16	80.64	0.45	35.13	0.35	37.63	0.48	35.19	2.34	83.24	0.33
Gd_2O_3	8.74	0.15	4.39	0.05	4.48	0.18	0.00	0.00	8.87	0.36	3.66	0.43	4.30	0.64	0.00	0.00
HfO_2	10.56	0.55	6.04	1.06	39.23	0.52	14.52	0.10	10.36	0.42	5.93	0.33	42.14	4.56	14.32	0.86
ThO_2	9.33	0.31	21.28	1.74	1.27	0.04	0.03	0.05	9.55	0.76	22.58	2.42	1.39	0.03	0.00	0.00
UO_2	19.96	0.71	26.63	2.60	4.17	0.13	1.08	0.11	21.11	0.55	26.03	1.46	3.76	0.41	0.86	0.05
Total	96.53	-	96.72	-	98.86	-	96.64	-	97.29	-	96.62	-	99.69	-	98.59	-
Al	0.010	0.001	0.021	0.003	0.124	0.004	0.004	0.000	0.006	0.003	0.014	0.001	0.134	0.012	0.002	0.001
Ca	1.028	0.007	0.074	0.015	0.956	0.009	0.002	0.001	0.999	0.008	0.052	0.004	0.941	0.007	0.001	0.001
Ti	2.013	0.016	1.938	0.024	1.944	0.017	0.926	0.002	2.019	0.007	1.971	0.012	1.903	0.072	0.933	0.003
Gd	0.220	0.003	0.101	0.002	0.106	0.005	0.000	0.000	0.225	0.010	0.084	0.010	0.102	0.009	0.000	0.000
Hf	0.229	0.012	0.119	0.020	0.778	0.021	0.064	0.001	0.226	0.008	0.118	0.006	0.835	0.087	0.062	0.003
Th	0.162	0.005	0.335	0.024	0.023	0.006	0.000	0.000	0.166	0.013	0.358	0.040	0.022	0.001	0.000	0.000
U	0.338	0.011	0.411	0.044	0.068	0.006	0.004	0.000	0.359	0.010	0.403	0.020	0.061	0.005	0.003	0.000
Catatoms	4.000	0.000	3.000	0.000	4.000	0.000	1.000	0.000	4.000	0.000	3.000	0.000	4.000	0.000	1.000	0.000
oxygen	6.857	-	5.865	-	6.929	-	1.996	-	6.885	-	5.899	-	6.940	-	1.998	-
Ca	0.000		0.000		0.956		0.000		0.000		0.000		0.941		0.000	
Gd	0.000		0.000		0.044		0.000		0.000		0.000		0.059		0.000	
Th	0.000		0.000		0.000		0.000		0.000		0.000		0.000		0.000	
Sum	0.000		0.000		1.000		0.000		0.000		0.000		1.000		0.000	
Charge	0.000		0.000		2.044		0.000		0.000		0.000		2.059		0.000	
Ca	1.028		0.074		0.000		0.000		0.999		0.052		0.000		0.000	
Al	0.010		0.000		0.068		0.000		0.006		0.000		0.037		0.000	
Gd	0.220		0.101		0.062		0.000		0.225		0.084		0.044		0.000	
Hf	0.229		0.079		0.778		0.000		0.226		0.102		0.835		0.000	
Th	0.162		0.335		0.023		0.000		0.166		0.358		0.022		0.000	
U	0.338		0.411		0.068		0.000		0.359		0.403		0.061		0.000	
Sum	1.987		1.000		1.000		0.000		1.981		1.000		1.000		0.000	
Charge	5.948		4.021		4.012		0.000		5.925		4.014		4.038		0.000	
Ti	2.013		1.938		1.944		0.926		2.019		1.971		1.903		0.933	
Hf	0.000		0.040		0.000		0.064		0.000		0.015		0.000		0.062	
Al	0.000		0.021		0.056		0.004		0.000		0.014		0.097		0.002	
Sum	2.013		2.000		2.000		0.994		2.019		2.000		2.000		0.996	
Charge	8.052		7.979		7.997		3.972		8.075		7.986		7.997		3.982	
UO_4	2.425		2.330		3.042		2.000		2.320		2.250		2.970		2.000	
Total Cations	4.000		3.000		4.000		0.994		4.000		3.000		4.000		0.996	
Model Oxygens	7.000		6.000		7.000		1.986		7.000		6.000		7.000		1.991	

Table 5. (cont.) Electron probe results and structural formulae for Th-analog experiments

	8-9 log fO_2 =-6.83								8-7 log fO_2 =-8					
	Pyrochlore	7	Brannerite	4	Hafnolite	3	Rutile	3	Pyrochlore	8	Brannerite	4	Rutile	4
	wt%	std dev	wt%	std dev	wt%	std dev	wt%	std dev	wt%	std dev	wt%	std dev	wt%	std dev
Al_2O_3	0.09	0.01	0.19	0.02	1.92	0.02	0.24	0.02	0.11	0.01	0.17	0.01	0.25	0.01
CaO	11.78	0.23	0.50	0.04	11.23	0.22	0.01	0.02	11.48	0.13	0.23	0.01	0.00	0.00
TiO_2	34.92	0.31	37.74	0.34	36.47	0.56	82.80	0.40	34.84	0.21	37.14	0.25	83.38	0.30
Gd_2O_3	8.30	0.14	3.15	0.18	4.91	0.34	0.00	0.00	8.47	0.20	2.41	0.05	0.00	0.00
HfO_2	10.82	0.28	6.52	0.78	38.68	1.04	14.58	0.81	10.69	0.16	6.30	0.34	14.06	0.16
ThO_2	10.18	0.24	22.18	0.81	1.66	0.07	0.00	0.00	10.70	0.45	23.10	1.60	0.00	0.00
UO_2	20.50	0.45	27.13	0.18	4.13	0.10	0.44	0.00	21.18	0.72	28.09	1.21	0.24	0.07
Total	96.58	-	97.40	-	98.98	-	98.07	-	97.46	-	97.43	-	97.94	-
Al	0.008	0.001	0.016	0.001	0.164	0.009	0.004	0.000	0.010	0.001	0.014	0.001	0.004	0.000
Ca	0.976	0.018	0.041	0.003	0.930	0.009	0.001	0.001	0.953	0.005	0.019	0.001	0.000	0.000
Ti	2.031	0.011	1.972	0.012	1.912	0.041	0.932	0.002	2.030	0.017	1.971	0.012	0.935	0.001
Gd	0.213	0.003	0.072	0.004	0.113	0.005	0.000	0.000	0.218	0.006	0.057	0.002	0.000	0.000
Hf	0.239	0.007	0.129	0.016	0.792	0.030	0.062	0.002	0.236	0.002	0.127	0.007	0.060	0.001
Th	0.179	0.004	0.351	0.012	0.026	0.002	0.000	0.000	0.189	0.007	0.371	0.024	0.000	0.000
U	0.353	0.008	0.419	0.004	0.063	0.003	0.002	0.000	0.365	0.012	0.441	0.019	0.001	0.000
Catatoms	4.000	0.000	3.000	0.000	4.000	0.000	1.000	0.000	4.000	0.000	3.000	0.000	1.000	0.000
oxygen	6.913	-	5.915	-	6.931	-	1.997	-	6.933	-	5.945	-	1.998	-
Ca	0.000		0.000		0.930		0.000		0.000		0.000		0.000	
Gd	0.000		0.000		0.070		0.000		0.000		0.000		0.000	
Th	0.000		0.000		0.000		0.000		0.000		0.000		0.000	
Sum	0.000		0.000		1.000		0.000		0.000		0.000		0.000	
Charge	0.000		0.000		2.070		0.000		0.000		0.000		0.000	
Ca	0.976		0.041		0.000		0.000		0.953		0.019		0.000	
Al	0.008		0.000		0.075		0.000		0.010		0.000		0.000	
Gd	0.213		0.072		0.043		0.000		0.218		0.057		0.000	
Hf	0.239		0.116		0.792		0.000		0.236		0.112		0.000	
Th	0.179		0.351		0.026		0.000		0.189		0.371		0.000	
U	0.353		0.419		0.063		0.000		0.365		0.441		0.000	
Sum	1.969		1.000		1.000		0.000		1.970		1.000		0.000	
Charge	5.874		4.016		4.018		0.000		5.881		4.014		0.000	
Ti	2.031		1.972		1.912		0.932		2.030		1.971		0.935	
Hf	0.000		0.013		0.000		0.062		0.000		0.015		0.060	
Al	0.000		0.016		0.088		0.004		0.000		0.014		0.004	
Sum	2.031		2.000		2.000		0.998		2.030		2.000		0.999	
Charge	8.126		7.984		7.997		3.987		8.119		7.986		3.992	
UO_2	2.247		2.203		3.088		2.000		2.183		2.124		2.000	
Total Cations	4.000		3.000		4.000		0.998		4.000		3.000		0.999	
Model Oxygens	7.000		6.000		7.000		1.993		7.000		6.000		1.996	

Table 5. (cont.) Electron probe results and structural formulae for Th-analog experiments

	8-8 $\log fO_2$ =10.06							
	Pyrochlore	6	Brannerite	3	*Hafnolite*	4	Rutile	3
	wt%	std dev	wt%	std dev	wt%	std dev	wt%	std dev
Al_2O_3	0.10	0.01	0.09	0.01	1.84	0.42	0.36	0.05
CaO	10.85	0.10	0.14	0.02	10.09	0.20	0.03	0.03
TiO_2	34.68	0.24	36.85	0.21	38.00	0.21	82.86	0.26
Gd_2O_3	8.17	0.28	1.46	0.07	5.38	0.15	0.00	0.00
HfO_2	10.51	0.19	6.14	0.31	34.92	0.75	14.58	0.55
ThO_2	11.04	0.27	23.66	1.92	2.73	0.28	0.00	0.00
UO_2	21.66	0.43	29.44	1.27	5.03	0.28	0.14	0.04
Total	97.02	-	97.78	-	98.00	-	97.97	-
Al	0.009	0.001	0.008	0.001	0.157	0.035	0.006	0.001
Ca	0.914	0.006	0.012	0.002	0.786	0.017	0.000	0.000
Ti	2.051	0.008	1.972	0.010	2.077	0.017	0.931	0.001
Gd	0.213	0.007	0.034	0.002	0.130	0.003	0.000	0.000
Hf	0.236	0.005	0.125	0.006	0.724	0.016	0.062	0.002
Th	0.198	0.005	0.383	0.031	0.045	0.004	0.000	0.000
U	0.379	0.006	0.466	0.020	0.081	0.004	0.000	0.000
Catatoms	4.000	0.000	3.000	0.000	4.000	-	1.000	0.000
oxygen	6.975	-	5.967	-	7.071	-	1.996	-
Ca	0.000		0.000		0.786		0.000	
Gd	0.000		0.000		0.130		0.000	
Th	0.000		0.000		0.000		0.000	
Sum	0.000		0.000		0.915		0.000	
Charge	0.000		0.000		1.960		0.000	
Ca	0.914		0.012		0.000		0.000	
Al	0.009		0.000		0.157		0.000	
Gd	0.213		0.034		0.000		0.000	
Hf	0.236		0.104		0.724		0.000	
Th	0.198		0.383		0.045		0.000	
U	0.379		0.466		0.081		0.000	
Sum	1.949		1.000		1.008		0.000	
Charge	5.796		4.008		3.875		0.000	
Ti	2.051		1.972		2.077		0.931	
Hf	0.000		0.020		0.000		0.062	
Al	0.000		0.008		0.000		0.006	
Sum	2.051		2.000		2.077		0.999	
Charge	8.204		7.992		8.306		3.990	
UO_2	2.067		2.071		2.000		2.000	
Total Cations	4.000		3.000		4.000		0.999	
Model Oxygens	7.000		6.000		7.071		1.995	

The composition of pyrochlore changes systematically with fO_2 and displays no composition discontinuities at the "hafnolite-in" boundaries (Figure 9); the regression coefficients with respect to log fO_2 are given in Table 8. The Hf and Gd concentrations are essentially constant (at the 2δ level) for all runs, but the Ca content of pyrochlore decreases with fO_2 in much the same way as it did in the Ce-analog experiments. However, unlike the Ce-analog the concentration of uranium is constant with respect to changing fO_2. The decrease in Ca is compensated by Ti and Th which both increase with decreasing fO_2 (Figure 10). The number of formula oxygen atoms per 4 cations in pyrochlore also increases with decreasing fO_2 as it did in the Ce-analog (Figure 9b). Since there is no cerium in these samples, the only valence change possible for accommodating this non-stoichiometry is $U^{+4} \leftrightarrow U^{+5,+6}$.

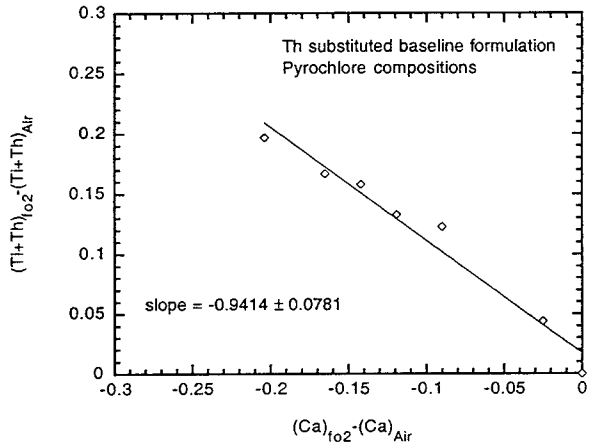

Figure 10. The variation in Ti + Th in pyrochlores sintered under reducing conditions relative to those sintered in air as a function of the change in Ca in runs sintered under reducing conditions relative to those sintered in air.

Brannerite compositions also vary systematically and continuously with decreasing fO_2, with the concentrations of Hf and Ca decreasing and U and Th concentrations and the model oxygen stoichiometry increasing (Figure 11). The increasing concentrations of U at lower fO_2s is consistent with the stabilization of brannerite under more reducing conditions.

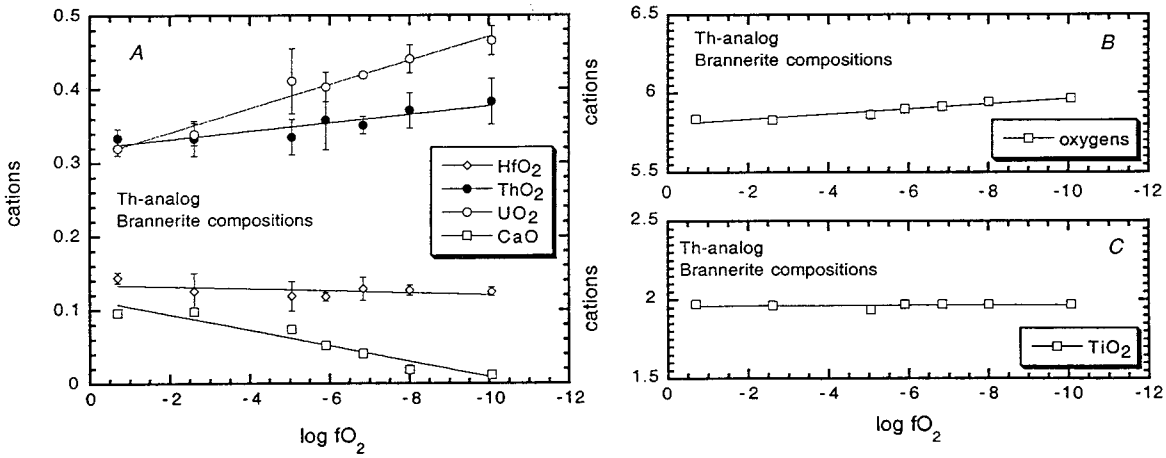

Figure 11. (A) Cation concentrations (normalized to 4 cations) in brannerite as a function of oxygen fugacity for the Th-analog mixture. (B) Oxygen concentration assuming quadravalent U. (C) Ti concentration (normalized to 4 cations) in pyrochlores as a function of oxygen fugacity for the Th-analog mixture.

The range of hafnolite compositions is smaller than that observed for brannerite and pyrochlore, but like that in the other phases varies systematically and continuously with fO_2 (Figure 12). Ti, Hf and U are all essentially constant with changing fO_2. The major chemical variations are in Th and Gd which increase (Th more strongly than Gd) and in Ca which decreases. For the run conducted in air, the "A" site in hafnolite (ABT_2O_7) is essentially filled with calcium (~0.97 Ca) and decreases with fO_2. If Th preferentially enters the "B" site, then the compositional trends

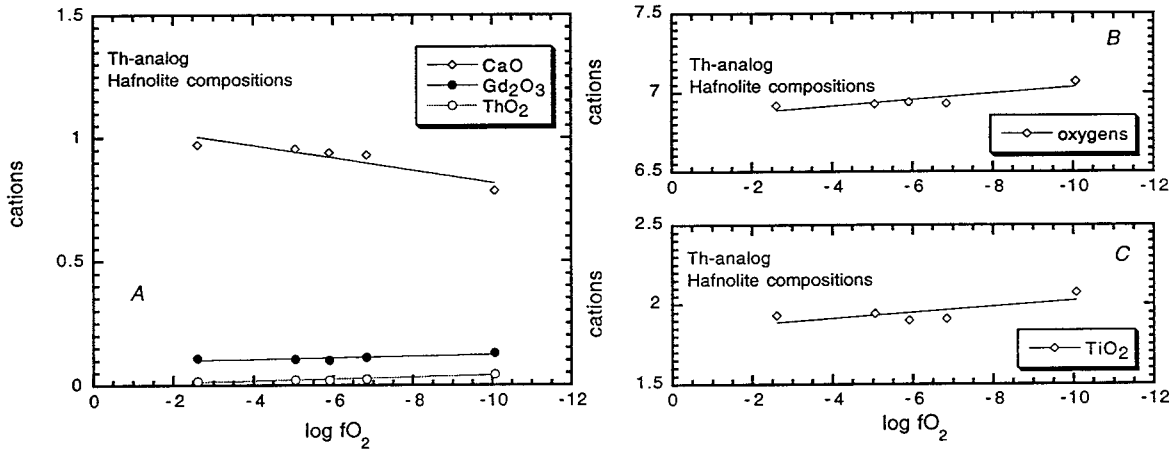

Figure 12. (A) Cation concentrations (normalized to 4 cations) in hafnolite as a function of oxygen fugacity for the Th-analog mixture. (B) Oxygen concentration assuming quadravalent U. (C) Ti concentration (normalized to 4 cations) in hafnolite as a function of oxygen fugacity for the Th-analog mixture

observed suggest that Gd is also accommodated on the B-site at high fO_2, and is displaced by increased Th concentration, moving to the A-site at lower fO_2. Otherwise, the hafnolites approach ideal ABT_2O_7 stoichiometry with charge excess on the A and B sites compensating for charge deficiency on the T-site (Table 5). The concentration of uranium in the hafnolites is sufficiently small as to have negligible effect on this conclusion.

Another feature of the hafnolite chemistry that should be noted is the presence of Al_2O_3 that reaches as high as 1.9 wt% in one experiment (8/9, Table 5). No Al_2O_3 was specifically added to

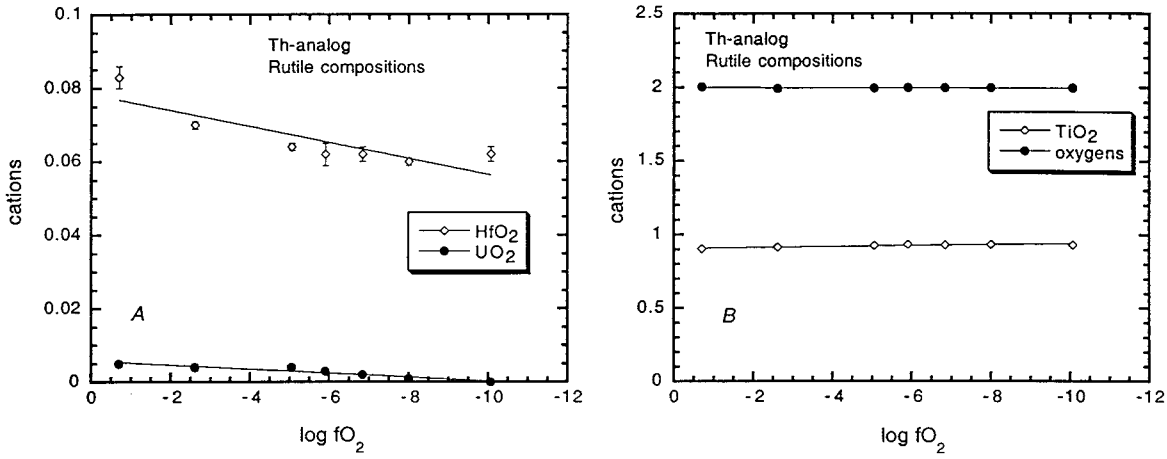

Figure 13. (A) Cation concentrations (normalized to 1 cation) in rutile as a function of oxygen fugacity for the Th-analog mixture. (B) Oxygen and titanium concentration (normalized to 1 cation) assuming quadravalent U.

the formulation, so it is probable that it is present as a processing contaminant added during grinding in an alumina mortar. Nevertheless, it has been previously observed that aluminum tends to stabilize hafnolite, and the presence of hafnolite in these runs may be partially attributed to this (Ryerson *et al.*, 2000).

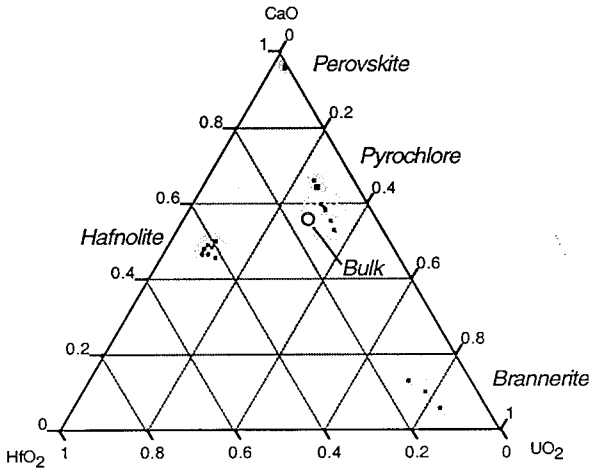

Figure 14. CaO-HfO_2-UO_2 diagram showing the compositions of perovskite, pyrochlore, hafnolite and brannerites from Ce/Al-analog materials sintered at 1350°C. Pyrochlores become richer in uranium with decreasing fO_2. The bulk composition is given by the open circle.

Rutiles from the Th-analog experiments are, within error, stoichiometric (Table 7). The UO_2 concentrations vary from ~0.2 to ~1.5 wt%, but ThO_2 concentrations are always close to the level of detection. The trends in chemistry are qualitatively identical to those observed in the Ce-analog; Hf and U both decrease with fO_2, correlated with an increase in Ti (Figure 13). The release of Hf and U from rutile is in some part responsible for the stabilization of hafnolite, and the increased U in brannerite (Figure 11), respectively.

4.3 Cerium-substituted analog with 10 wt% Al_2O_3

The phase assemblages in the cerium-substituted analog with 10 wt% Al_2O_3 (hereafter referred to as the Ce/Al analog) bear some similarity to those in the Ce-analog runs. However, the effects

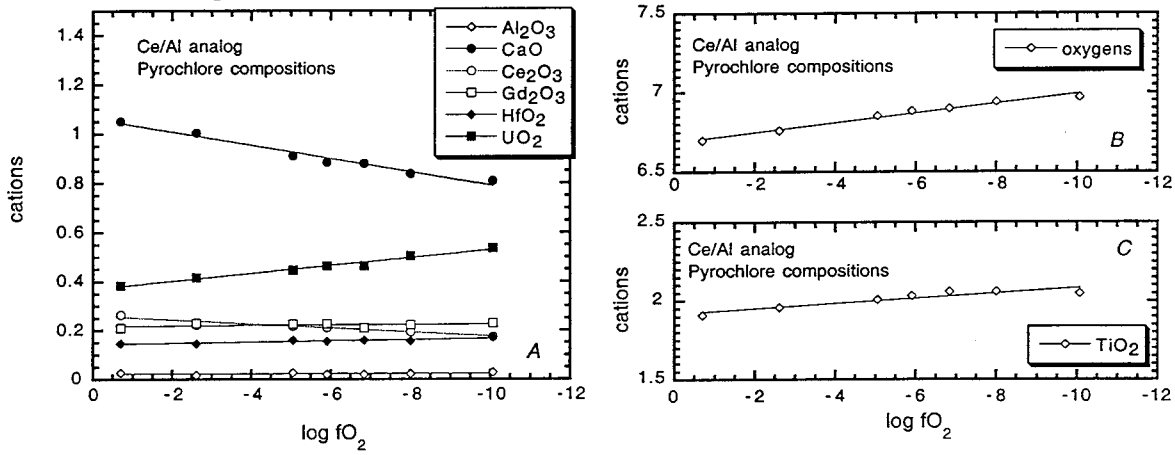

Figure 15. (A) Cation concentrations (normalized to 4 cations) in pyrochlore as a function of oxygen fugacity for the Ce/Al-analog mixture. (B) Oxygen concentration assuming trivalent Ce and quadravalent U. (C) Ti concentration (normalized to 4 cations) in pyrochlore as a function of oxygen fugacity for the Ce/Al-analog mixture.

of Al_2O_3 addition are observed in both the stabilization of hafnolite (with typical Al_2O_3 concentrations are 4-6 wt%) and in the presence of Al-rich accessory phases (Table 3). At high fO_2 Al-psuedobrookite (nominally Al_2TiO_5) is the stable Al-rich phase. As fO_2 is decreased the Al-rich phase becomes a calcium-titanoaluminate with the nominal formula $AT_{11}O_{19}$ where the

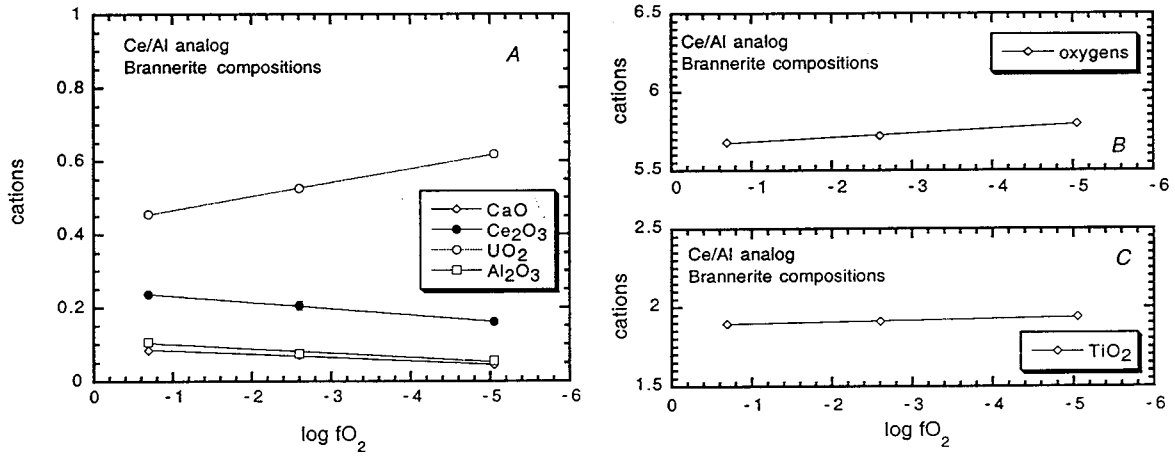

Figure 16. (A) Cation concentrations (normalized to 4 cations) in brannerite as a function of oxygen fugacity for the Ce/Al-analog mixture. (B) Oxygen concentration assuming trivalent Ce and quadravalent U. (C) Ti concentration (normalized to 4 cations) in brannerite as a function of oxygen fugacity for the Ce/Al-analog mixture.

"A" site is filled with Ca and Ce and the T-site with Al (~9 cations) and Ti (~2 cations). At fO_2s more oxidizing than log fO_2=-5.05 brannerite is present and at fO_2s more reducing than log fO_2=-6.83 perovskite is present (Table 3).

The pyrochlores form an array parallel to the CaO-UO_2 join on the CaO-HfO_2-UO_2 ternary (Figure 14) becoming enriched in UO_2 as fO_2 decreases, as in the Ce- and Th-analog experiments. The variation in chemistry is also similar to that observed in the other analog materials (Table 6). As fO_2 decreases the Ca and Ce contents of the pyrochlores decrease, and the U and Ti concentrations increase (Figure 15). Assuming Ce^{+3} and U^{+4}, the total oxygen atom contents increases to close to the ideal content with decreasing fO_2 (Figure 15b).

Brannerite plots at a constant Ca/Hf ratio on the CaO-HfO_2-UO_2 ternary (Figure 14) becoming richer in UO_2 as fO_2 decreases (Figure 16). Hafnolite forms a relatively tight cluster on the CaO-HfO_2-UO_2 ternary (Figure 14), and are close to the ideal 4 cations to 6 oxygen stoichiometry (Table 6). The chemistry does show systematic variations with fO_2, however, as Ca and Hf

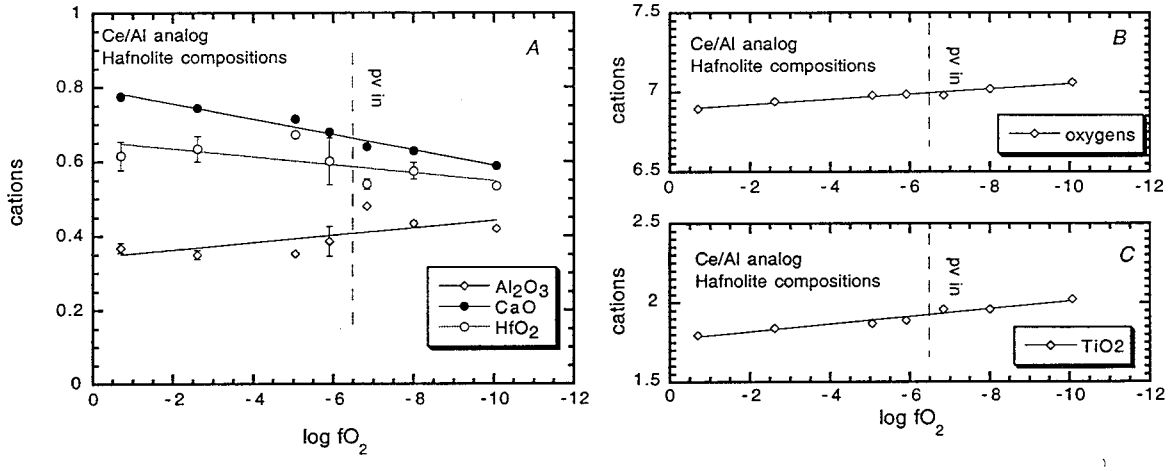

Figure 17. (A) Cation concentrations (normalized to 4 cations) in hafnolite as a function of oxygen fugacity for the Ce/Al-analog mixture. (B) Oxygen concentration assuming trivalent Ce and quadravalent U. (C) Ti concentration (normalized to 4 cations) in hafnolite as a function of oxygen fugacity for the Ce/Al-analog mixture.

decrease with decreasing fO_2 and Al and Ti increase (Figure 17). Perovskite is strongly enriched in cerium (up to 23 wt% Ce_2O_3) and displays limited compositional variation (Figure 14). Oxygen in excess of the ideal 3 oxygens normalized to 2 cations are observed (Table 6), indicating the existence of cation vacancies in perovskite.

Psuedobrookite is observed in the run sintered in air, and is essentially free of all elements other than Al and Ti (7-3, Table 7). The calcium-titanoaluminate, on the otherhand, does incorporate cerium (typical concentrations are ~7 wt% Ce_2O_3), and to a lesser extent gadolinium, hafnium and uranium. If cerium is, indeed, a good analog for plutonium, we would expect this calcium-aluminotitanate phase to incorporate Pu in the actual Pu-bearing baseline formulation fabricated under these conditions.

As in the Ce-analog, the major compositional variations observed are the decreases in Ca and Ce in pyrochlore, brannerite and hafnolite under more reducing conditions. The progressive release of these components can be seen in the changing phase assemblage. The first manifestation is the reaction of Ca and Ce with psuedobrookite to yield the calcium-titanoaluminate phase that incorporates both of these components. As conditions become more reducing Ca and Ce react with, and destabilize brannerite producing perovskite and progressively more UO_2-rich pyrochlore.

Table 6. Electron probe results and structural formulas of the Ce/Al analog experiments

	7-3 $\log fO_2$ = -0.69								7-4 $\log fO_2$ = -2.6									
	Pyrochlore	4	Brannerite	3	Hafnolite	3	Psb	2	Pyrochlore	6	Hafnolite	5	Brannerite	5	CTA	4	Rutile	3
	wt%	std dev	wt%	std dev	wt%	std dev	wt%	std dev	wt%	std dev	wt%	std dev	wt%	std dev	wt%	std dev	wt%	std dev
Al_2O_3	0.32	0.01	1.44	0.05	4.35	0.18	42.09	2.11	0.20	0.04	4.08	0.16	0.98	0.01	65.59	10.56	1.12	0.08
CaO	13.41	0.11	1.25	0.05	10.13	0.54	0.00	0.00	12.49	0.16	9.52	0.18	1.02	0.04	3.28	0.90	0.09	0.00
TiO_2	34.77	0.35	40.27	0.09	33.43	0.11	0.00	0.00	34.73	0.24	33.61	0.19	39.21	0.18	22.28	5.98	83.24	0.68
Ce_2O_3	9.89	0.35	10.28	0.18	4.25	0.56	0.00	0.00	8.11	0.24	3.58	0.24	8.65	0.51	7.86	2.14	0.11	0.01
Gd_2O_3	8.72	0.22	6.30	0.24	7.40	0.40	0.00	0.00	9.26	0.28	7.49	0.16	6.10	0.21	0.78	0.26	0.04	0.05
HfO_2	7.10	0.07	5.08	0.13	30.43	2.36	98.85	0.33	6.83	0.12	30.45	1.67	4.32	0.09	0.88	0.30	11.65	0.35
UO_2	23.62	0.72	32.68	0.26	9.55	1.41	0.00	0.00	24.96	0.34	9.41	0.96	36.46	0.53	0.38	0.51	2.87	0.04
Total	97.83	-	97.30	-	99.52	-	0.00	0.00	96.58	-	98.14	-	96.75	-	101.05	2.38	99.13	0.94
Al	0.028	0.001	0.107	0.004	0.368	0.013	2.036	0.053	0.018	0.004	0.350	0.012	0.075	0.001	9.141	0.913	0.018	0.002
Ca	1.051	0.005	0.084	0.003	0.775	0.025	0.001	0.001	1.005	0.008	0.744	0.014	0.071	0.003	0.423	0.136	0.002	0.001
Ti	1.912	0.013	1.897	0.002	1.799	0.006	0.964	0.053	1.961	0.007	1.843	0.008	1.912	0.008	2.018	0.635	0.920	0.001
Ce	0.265	0.008	0.236	0.003	0.112	0.010	0.000	0.000	0.223	0.007	0.096	0.007	0.205	0.012	0.347	0.111	0.001	0.000
Gd	0.211	0.004	0.131	0.005	0.175	0.006	0.000	0.000	0.231	0.006	0.181	0.003	0.131	0.004	0.031	0.012	0.000	0.001
Hf	0.148	0.002	0.091	0.002	0.616	0.039	0.000	0.000	0.146	0.003	0.634	0.034	0.080	0.002	0.030	0.011	0.049	0.001
U	0.384	0.013	0.456	0.004	0.155	0.016	0.000	0.000	0.417	0.005	0.153	0.016	0.526	0.008	0.010	0.014	0.010	0.000
Catatoms	4.000	0.000	3.000	0.000	4.000	0.000	3.000	0.000	4.000	0.000	4.000	0.000	3.000	0.000	12.000	0.000	1.000	0.000
Oxygen	6.697	-	5.680	-	6.897	-	4.982	-	6.760	-	6.943	-	5.723	-	18.818	-	1.988	-
$Ce^{+4}/\sum Ce$	0.330		0.330		0.330		0.000		0.263		0.263		0.263		0.000		0.000	
Ca	0.000		0.000		0.775		0.000		0.000		0.744		0.000		0.000		0.000	
Gd	0.000		0.000		0.175		0.000		0.000		0.181		0.000		0.000		0.000	
Ce^{+3}	0.000		0.000		0.075		0.000		0.000		0.071		0.000		0.000		0.000	
Ce^{+4}	0.000		0.000		0.037		0.000		0.000		0.025		0.000		0.000		0.000	
Sum	0.000		0.000		1.025		0.000		0.000		0.995		0.000		0.000		0.000	
Charge	0.000		0.000		2.448		0.000		0.000		2.343		0.000		0.000		0.000	
Ca	1.051		0.084		0.000		0.001		1.005		0.000		0.071		0.423		0.000	
Al	0.000		0.004		0.167		2.036		0.000		0.193		0.000				0.000	
Ce^{+3}	0.177		0.158		0.037		0.000		0.164		0.025		0.151		0.347		0.000	
Ce^{+4}	0.087		0.078		0.000		0.000		0.059		0.000		0.054				0.000	
Gd	0.211		0.131		0.000		0.000		0.231		0.000		0.131		0.031		0.000	
Hf	0.089		0.091		0.616		0.000		0.125		0.634		0.066		0.030		0.000	
U	0.384		0.456		0.155		0.000		0.417		0.153		0.526		0.010		0.000	
Sum	2.000		1.000		0.975		2.036		2.000		1.005		1.000		0.842		0.000	
Charge	6.028		4.114		4.628		6.108		6.018		4.706		4.075		2.142		0.000	
Ti	1.912		1.897		1.799		0.964		1.961		1.843		1.912		2.018		0.920	
Hf	0.060		0.000		0.000		0.000		0.021		0.000		0.014		0.000		0.049	
Al	0.028		0.103		0.201		0.014		0.018		0.157		0.075		9.141		0.018	
Sum	2.000		2.000		2.000		0.978		2.000		2.000		2.000		11.158		0.987	
Charge	7.972		7.897		7.799		3.897		7.982		7.843		7.925		35.493		3.931	
UO_x	2.675		2.629		2.186		2.000		2.506		2.046		2.475		2.000		3.950	
Total	4.000		3.000		4.000		3.014		4.000		4.000		3.000		12.000		0.987	
Model Oxygens	7.000		6.000		7.000		5.003		7.000		7.000		6.000		18.818		1.975	

Table 6. (cont,) Electron probe results and structural formulas of the Ce/Al analog experiments

	7-5 $\log fO_2$ = -5.05										7-6 $\log fO_2$ = -5.9							
	Pyrochlore	5	Hafnolite	5	Brannerite	5	CTA	3	Rutile	4	Pyrochlore	6	Hafnolite	12	CTA	4	Rutile	4
	wt%	std dev	wt%	std dev	wt%	std dev	wt%	std dev	wt%	std dev	wt%	std dev	wt%	std dev	wt%	std dev	wt%	std dev
Al_2O_3	0.30	0.08	4.16	0.04	0.69	0.02	69.54	7.46	0.66	0.15	0.24	0.01	4.69	0.59	58.47	1.41	0.87	0.18
CaO	11.24	0.15	9.25	0.07	0.62	0.03	2.80	0.64	0.12	0.03	11.11	0.14	9.04	0.31	3.79	0.19	0.14	0.11
TiO_2	35.30	0.22	34.49	0.37	38.48	0.10	19.61	4.52	85.31	0.55	36.27	0.24	36.88	1.82	26.39	0.82	86.37	1.08
Ce_2O_3	7.85	0.35	3.53	0.21	6.55	0.20	7.72	1.95	0.03	0.03	7.77	0.14	4.01	0.41	10.31	0.51	0.17	0.08
Gd_2O_3	9.01	0.22	6.75	0.29	4.48	0.03	0.57	0.23	0.04	0.02	9.23	0.16	7.41	0.79	0.74	0.10	0.12	0.07
HfO_2	7.46	0.13	32.69	0.36	4.26	0.08	1.03	0.41	10.76	0.16	7.33	0.13	30.05	2.49	1.08	0.09	10.85	0.34
UO_2	26.58	0.26	8.25	0.22	41.51	0.70	0.37	0.38	1.83	0.12	27.96	0.13	7.71	0.77	0.54	0.46	1.51	0.05
Total	97.74	-	99.10	-	96.57	-	101.62	0.44	98.76	0.35	99.92	-	99.78	0.44	101.32	0.26	100.03	1.04
Al	0.027	0.007	0.353	0.003	0.055	0.002	9.524	0.664	0.012	0.004	0.021	0.001	0.386	0.040	8.439	0.069	0.014	0.003
Ca	0.911	0.011	0.715	0.005	0.044	0.002	0.351	0.091	0.002	0.001	0.885	0.010	0.679	0.038	0.514	0.013	0.002	0.001
Ti	2.009	0.011	1.871	0.011	1.940	0.008	1.727	0.451	0.935	0.004	2.034	0.010	1.940	0.052	2.491	0.050	0.933	0.003
Ce	0.218	0.010	0.093	0.005	0.161	0.004	0.331	0.094	0.000	0.000	0.212	0.003	0.103	0.009	0.470	0.027	0.001	0.000
Gd	0.226	0.006	0.161	0.007	0.100	0.001	0.022	0.010	0.000	0.000	0.227	0.003	0.172	0.015	0.029	0.004	0.001	0.000
Hf	0.161	0.003	0.673	0.007	0.081	0.001	0.034	0.015	0.045	0.001	0.156	0.003	0.601	0.063	0.038	0.004	0.044	0.001
U	0.448	0.005	0.132	0.004	0.619	0.009	0.010	0.010	0.006	0.000	0.465	0.005	0.120	0.015	0.018	0.013	0.005	0.000
Catatoms	4.000	0.000	4.000	0.000	3.000	0.000	12.000	0.000	1.000	0.000	4.000	0.000	4.000	0.000	12.000	0.000	1.000	0.000
Oxygen	6.853	-	6.981	-	5.798	-	18.710	-	1.992	-	6.885	-	6.991	0.009	19.017	-	1.990	-
$Ce^{+4}/\Sigma Ce$	0.176		0.176		0.176		0.000		0.000		0.147		0.147		0.000		0.000	
Ca	0.000		0.715		0.000		0.000		0.000		0.000		0.679		0.000		0.000	
Gd	0.000		0.161		0.000		0.000		0.000		0.000		0.172		0.000		0.000	
Ce^{+3}	0.000		0.077		0.000		0.000		0.000		0.000		0.088		0.000		0.000	
Ce^{+4}	0.000		0.016		0.000		0.000		0.000		0.000		0.015		0.000		0.000	
Sum	0.000		0.953		0.000		0.000		0.000		0.000		0.938		0.000		0.000	
Charge	0.000		2.210		0.000		0.000		0.000		0.000		2.195		0.000		0.000	
Ca	0.911		0.000		0.044		0.351		0.000		0.885		0.000		0.514		0.000	
Al	0.027		0.225		0.000		0.000		0.000		0.021		0.325		0.000		0.000	
Ce^{+3}	0.179		0.016		0.132		0.331		0.000		0.181		0.015		0.470		0.000	
Ce^{+4}	0.038		0.000		0.028		0.000		0.000		0.031		0.000		0.000		0.000	
Gd	0.226		0.000		0.100		0.022		0.000		0.227		0.000		0.029		0.000	
Hf	0.161		0.673		0.076		0.034		0.000		0.156		0.601		0.038		0.000	
U	0.448		0.132		0.619		0.010		0.000		0.465		0.120		0.018		0.000	
Sum	1.991		1.047		1.000		0.748		0.000		1.966		1.062		1.070		0.000	
Charge	6.045		4.889		4.055		1.938		0.000		5.929		5.164		2.753		0.000	
Ti	2.009		1.871		1.940		1.727		0.935		2.034		1.940		2.491		0.933	
Hf	0.000		0.000		0.005		0.000		0.045		0.000		0.000		0.000		0.044	
Al	0.000		0.129		0.055		9.524		0.012		0.000		0.060		8.439		0.014	
Sum	2.009		2.000		2.000		11.252		0.992		2.034		2.000		10.930		0.991	
Charge	8.036		7.871		7.945		35.482		3.955		8.135		7.940		35.281		3.950	
UO_2	2.375		1.894		2.303		2.000		2.000		2.283		1.822		2.000		2.000	
Total	4.000		4.000		3.000		12.000		0.992		4.000		4.000		12.000		0.991	
Model	7.000		7.000		6.000		18.710		1.975		7.000		7.000		19.017		1.975	
Oxygens																		

Table 6. (cont,) Electron probe results and structural formulas of the Ce/Al analog experiments

	7-9 $\log fO_2$ = -6.83								7-7 $\log fO_2$ = -8.00							
	Pyrochlore	6	Hafnolite	6	Perovskite	6	CTA	4	Pyrochlore	6	Hafnolite	6	Perovskite	6	CTA	4
	wt%	std dev	wt%	std dev	wt%	std dev	wt%	std dev	wt%	std dev	wt%	std dev	wt%	std dev	wt%	std dev
Al_2O_3	0.23	0.01	6.09	0.05	2.06	0.07	60.77	0.90	0.26	0.01	5.26	0.06	1.93	0.08	57.09	0.50
CaO	10.99	0.05	8.89	0.08	20.41	0.64	3.89	0.24	10.13	0.13	8.39	0.13	20.53	0.39	3.83	0.16
TiO_2	36.56	0.19	38.83	0.33	47.10	0.39	27.25	0.65	35.62	0.24	37.24	0.72	46.34	0.57	27.28	0.23
Ce_2O_3	7.50	0.21	4.30	0.20	23.48	1.45	10.44	0.37	6.91	0.10	4.17	0.24	23.01	1.13	10.74	0.46
Gd_2O_3	8.65	0.18	7.63	0.21	5.00	0.50	0.86	0.18	8.67	0.18	6.86	0.40	5.39	0.35	0.89	0.19
HfO_2	7.26	0.25	28.13	0.73	0.34	0.11	1.17	0.09	7.19	0.12	28.77	0.97	0.79	0.09	1.16	0.24
UO_2	27.92	0.23	7.66	0.12	1.99	0.12	0.83	0.25	29.48	0.45	8.58	0.19	2.39	0.16	0.52	0.63
Total	99.10	-	101.51	-	100.38	-	105.21	-	98.26	-	99.28	-	100.38	-	101.52	0.22
Al	0.020	0.001	0.480	0.004	0.069	0.002	8.518	0.105	0.023	0.001	0.434	0.007	0.065	0.003	8.353	0.040
Ca	0.881	0.004	0.638	0.006	0.620	0.014	0.495	0.030	0.839	0.011	0.629	0.007	0.628	0.009	0.519	0.018
Ti	2.058	0.009	1.955	0.014	1.005	0.011	2.437	0.062	2.059	0.011	1.961	0.024	0.994	0.005	2.550	0.013
Ce	0.206	0.006	0.105	0.005	0.244	0.016	0.454	0.018	0.194	0.003	0.107	0.006	0.240	0.013	0.480	0.012
Gd	0.214	0.005	0.169	0.005	0.047	0.004	0.034	0.007	0.221	0.005	0.159	0.009	0.051	0.003	0.039	0.008
Hf	0.155	0.005	0.538	0.014	0.003	0.001	0.040	0.003	0.158	0.002	0.575	0.023	0.006	0.001	0.043	0.010
U	0.465	0.004	0.114	0.002	0.013	0.001	0.022	0.006	0.506	0.009	0.134	0.003	0.015	0.001	0.016	0.021
Catatoms	4.000	0.000	4.000	0.000	2.000	0.000	12.000	-	4.000	0.000	4.000	0.000	2.000	0.000	12.000	0.000
Oxygen	6.898	-	6.984	-	3.200	-	19.002	-	6.942	-	7.020	-	3.194	-	19.045	-
$Ce^{+4}/\Sigma Ce$	0.114		0.114		0.114		0.000		0.073		0.073		0.073		0.000	
Ca	0.000		0.638		0.000		0.000		0.000		0.762		0.000		0.000	
Gd	0.000		0.169		0.000		0.000		0.000		0.127		0.000		0.000	
Ce^{+3}	0.000		0.093		0.000		0.000		0.000		0.084		0.000		0.000	
Ce^{+4}	0.000		0.012		0.000		0.000		0.000		0.000		0.000		0.000	
Sum	0.000		0.901		0.000		0.000		0.000		0.973		0.000		0.000	
Charge	0.000		2.112		0.000		0.000		0.000		2.156		0.000		0.000	
Ca	0.881		0.000		0.620		0.495		0.839		0.000		0.628		0.519	
Al	0.020		0.436		0.069		0.000		0.023		0.183		0.065		0.000	
Ce^{+3}	0.182		0.012		0.244		0.454		0.180		0.000		0.223		0.480	
Ce^{+4}	0.023		0.000		0.000		0.000		0.014		0.000		0.017		0.000	
Gd	0.214		0.000		0.047		0.034		0.221		0.000		0.051		0.039	
Hf	0.155		0.538		0.000		0.040		0.158		0.769		0.006		0.043	
U	0.465		0.114		0.013		0.022		0.506		0.075		0.015		0.016	
Sum	1.942		1.099		0.993		1.045		1.941		1.027		1.006		1.097	
Charge	5.829		5.567		2.370		2.702		5.835		3.926		2.428		2.831	
Ti	2.058		1.955		1.005		2.437		2.059		1.996		0.994		2.550	
Hf	0.000		0.000		0.003		0.000		0.000		0.000		0.000		0.000	
Al	0.000		0.045		0.000		8.518		0.000		0.004		0.000		8.353	
Sum	2.058		2.000		1.007		10.955		2.059		2.000		0.994		10.903	
Charge	8.232		7.955		4.030		35.301		8.236		7.996		3.977		35.259	
UO_2	2.259		1.926		2.000		2.000		2.170		1.482		2.000		2.000	
Total	4.000		4.000		2.000		12.000		4.000		4.000		2.000		12.000	
Model Oxygens	7.000		7.000		3.200		19.002		7.000		7.000		3.203		19.045	

Table 6. (cont,) Electron probe results and structural formulas of the Ce/Al analog experiments

	7-8 $\log fO_2$ = -10.06							
	Pyrochlore	4	Hafnolite	4	Perovskite	4	CTA	4
	wt%	std dev	wt%	std dev	wt%	std dev	wt%	std dev
Al_2O_3	0.31	0.08	5.10	0.05	1.95	0.18	56.43	1.07
CaO	9.59	0.09	7.86	0.06	21.26	0.85	3.66	0.26
TiO_2	34.56	0.42	38.49	0.26	46.29	0.69	26.99	0.89
Ce_2O_3	6.07	0.07	3.80	0.10	21.54	1.30	10.27	0.60
Gd_2O_3	8.80	0.28	7.62	0.39	5.36	0.38	0.79	0.13
HfO_2	7.61	0.08	26.72	0.08	0.98	0.43	1.26	0.19
UO_2	30.64	0.57	10.04	0.07	3.21	0.21	0.37	0.22
Total	97.58	-	99.62	-	100.59	-	99.77	0.84
Al	0.029	0.007	0.420	0.005	0.065	0.006	8.383	0.167
Ca	0.810	0.007	0.589	0.004	0.646	0.020	0.493	0.043
Ti	2.048	0.019	2.026	0.011	0.987	0.010	2.545	0.107
Ce	0.175	0.002	0.097	0.002	0.224	0.015	0.484	0.023
Gd	0.230	0.007	0.177	0.009	0.050	0.004	0.034	0.005
Hf	0.171	0.002	0.534	0.002	0.008	0.004	0.048	0.006
U	0.537	0.011	0.156	0.001	0.020	0.001	0.012	0.006
Catatoms	4.000	0.000	4.000	0.000	2.000	0.000	12.000	0.000
Oxygen	6.973	-	7.063	-	3.185	-	19.056	-
$Ce^{+4}/\Sigma Ce$	0.000		0.000		0.000		0.000	
Ca	0.000		0.589		0.000		0.000	
Gd	0.000		0.177		0.000		0.000	
Ce^{+3}	0.000		0.097		0.000		0.000	
Ce^{+4}	0.000		0.000		0.000		0.000	
Sum	0.000		0.864		0.000		0.000	
Charge	0.000		2.002		0.000		0.000	
Ca	0.810		0.000		0.646		0.493	
Al	0.029		0.420		0.065		0.000	
Ce^{+3}	0.175		0.000		0.224		0.484	
Ce^{+4}	0.000		0.000		0.000		0.000	
Gd	0.230		0.000		0.050		0.034	
Hf	0.171		0.534		0.008		0.048	
U	0.537		0.156		0.020		0.012	
Sum	1.952		1.110		1.013		1.072	
Charge	5.897		5.448		2.422		2.782	
Ti	2.048		2.026		0.987		2.545	
Hf	0.000		0.000		0.000		0.000	
Al	0.000		0.000		0.000		8.383	
Sum	2.048		2.026		0.987		10.928	
Charge	8.191		8.103		3.948		35.330	
UO_x	2.132		6.562		2.000		2.000	
Total	4.000		1.596		2.000		12.000	
Model Oxygens	7.000		7.000		3.185		19.056	

Table 7. Mole fraction of pyrochlore components								
	$CaUTiAlO_7$	$CaTi_3O_7$	$Ce_2Ti_2O_7$	$Gd_2Ti_2O_7$	$CaHfTi_2O_7$	$CaThTi_2O_7$	$Ca_{1.5}U_{0.5}Ti_2O_7$	$CaUTi_2O_7$
Ce Analog								
1/3	0.015	*-0.061*	0.123	0.116	0.221	0.000	0.501	0.086
1/4	0.024	*-0.065*	0.122	0.119	0.221	0.000	0.417	0.163
1/5	0.011	0.027	0.119	0.113	0.216	0.000	0.238	0.277
1/6	0.011	0.046	0.117	0.111	0.215	0.000	0.212	0.289
1/9	0.011	0.058	0.112	0.112	0.224	0.000	0.148	0.336
1/7	0.009	0.065	0.105	0.116	0.232	0.000	0.103	0.371
1/8	0.009	0.088	0.098	0.118	0.224	0.000	0.034	0.430
Ce/Al Analog								
7/3	0.028	*-0.060*	0.133	0.106	0.148	0.000	0.579	0.067
7/4	0.018	*-0.021*	0.112	0.116	0.146	0.000	0.464	0.167
7/5	0.027	0.036	0.109	0.113	0.161	0.000	0.266	0.288
7/6	0.021	0.055	0.106	0.114	0.156	0.000	0.209	0.340
7/9	0.020	0.078	0.103	0.107	0.155	0.000	0.183	0.353
7/7	0.023	0.082	0.097	0.111	0.158	0.000	0.093	0.437
7/8	0.029	0.077	0.088	0.115	0.171	0.000	0.025	0.496
Th Analog								
8/3	0.000	*-0.091*	0.000	0.109	0.232	0.143	0.454	0.154
8/4	0.004	*-0.050*	0.000	0.110	0.240	0.149	0.405	0.143
8/5	0.010	0.023	0.000	0.110	0.229	0.162	0.276	0.190
8/6	0.006	0.025	0.000	0.113	0.226	0.166	0.223	0.242
8/9	0.008	0.040	0.000	0.107	0.239	0.179	0.166	0.262
8/7	0.010	0.040	0.000	0.109	0.236	0.189	0.124	0.293
8/8	0.009	0.060	0.000	0.107	0.236	0.198	0.041	0.350

5. Discussion

5.1 Oxidation states

As is the case with plutonium, cerium and uranium can both be present in more than a single valence state, and the distribution of each of these elements among the possible valence states will depend upon temperature, fO_2 and mineral chemistry. Due to the polyphase nature of the samples investigated here, the valence of these cations has not been directly determined by either spectroscopic or wet chemical methods. Instead, we present a simple model based upon the ideal stoichiometry of the phases in question coupled with spectroscopic determinations from other workers to constrain the range of possible valence state distributions. The major caveat is that these constraints depend upon the assumption of ideal stoichiometry; if any of the phases in question has significant concentrations of defects, then these constraints must be reevaluated and modified.

Pyrochlore and brannerite are oxygen deficient for stoichiometries based on Ce^{+3} and U^{+4} for each of the starting compositions (Table 4, 5, 6). For example, if uranium and cerium are assumed to be present as +4 and +3 cations, respectively, then the pyrochlore and brannerite from the Ce-Al analog run in air yield 6.7 and 5.7 oxygens for 4 and 3 cations, respectively (Table 6). Conversely, hafnolite approaches ideality in air, and perovskite is actually cation deficient. To achieve ideal pyrochlore and brannerite stoichiometry, either U or Ce, or some combination of these elements must exist in a higher valence state. Similarly in the Th-analog, where U is the only cation with multiple valence states, a run in air yields 6.8 and 5.8 oxygens for 4 and 3 cations for pyrochlore and brannerite, respectively (Table 5). If ideal stoichiometry is achieved in these phases, then the Th-analog runs require that at least some fraction of the uranium must be present in a valence state higher than +4. Comparison of the Ce-Al and Th-analog runs also indicates that the Th-analog runs produce samples slightly closer to ideal stoichiometry than the Ce-Al and Ce- runs. The simplest explanation is that Ce must also be present as both Ce^{+3} and

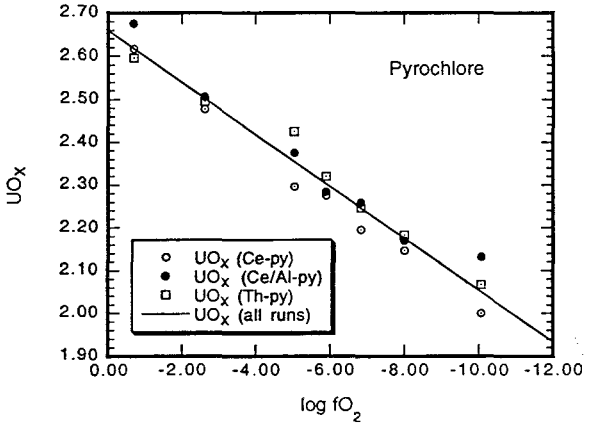

Figure 18. Average uranium oxidation state for pyrochlore as a function of log fO_2. The calculation assumes that $Ce^{+4}/\Sigma Ce=0.33$ in air, and 0 at log $fO_2=-10$. UO_x is then adjusted to produce ideal pyrochlore stoichiometry (see text).

Ce^{+4}. Mixed valences for Ce and U are supported by the work of Fortner *et al.* (1999), who determined the valence of Ce and U in a ceramic formulation similar to those presented here using XANES and EXAFS spectroscopy. They found that cerium exists in a mixed oxidation state ($Ce^{+4}/\sum Ce$ ~0.33) and that uranium is present largely as the pentavalent species (personal communication, 1999). Xu and Wang (1999) have also identified Ce^{+4} in natural pyrochlores by electron energy loss spectroscopy (EELS).

At the lowest fO_2s (log fO_2 =-10, runs 1/8, 7/8 and 8/8, Table 4, 5, 6) pyrochlore and brannerite are, within analytical error, stoichiometric based on Ce^{+3} and U^{+4} for each of the starting compositions. Hence, at fO_2s between air and log fO_2=-10, both uranium and cerium appear to be reduced from a mixed valence state to their lowest valence. To model the variation in valence state as a function of oxygen fugacity, we assume, following Fortner *et al.* (1999) that the $Ce^{+4}/\sum Ce$ for both pyrochlore and brannerite is 0.33 in air, and, consistent with our results, 0 at log fO_2=-10. Between these extremes, we assume that $Ce^{+4}/\sum Ce$ varies linearly with log fO_2 (see Table 4, 5, 6). By fixing the relationship between $Ce^{+4}/\sum Ce$ and fO_2, we can calculate the "average oxidation state" for uranium, UO_x (where x is the number of oxygens/uranium atom) based on the ideal 4/7 and 3/6 stoichiometries of pyrochlore and brannerite, respectively (see Tables 4, 5, 6). The "average valence" is obviously twice the average oxidation state, however, as various combinations of uranium valence states can satisfy the ideal stoichiometry, the result obtained is not unique, nor does it resolve the distribution of uranium among U^{+4}, U^{+5} and U^{+6}.

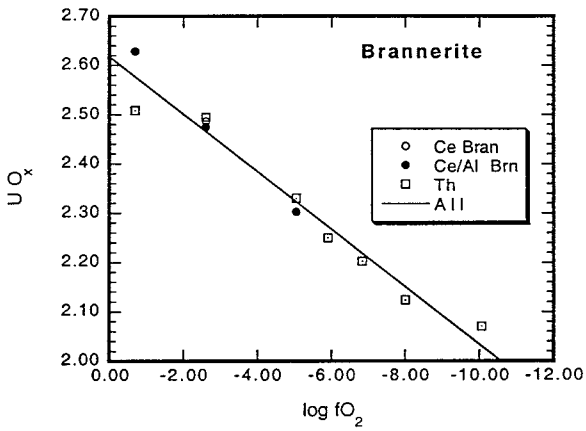

Figure 19. Average uranium oxidation state for brannerite as a function of log fO_2. The calculation assumes that $Ce^{+4}/\Sigma Ce$=0.33 in air, and 0 at log fO_2=-10. UO_x is then adjusted to produce ideal brannerite stoichiometry (see text).

The model uranium oxidation state for pyrochlores and brannerites from each of the starting compositions decreases linearly with log fO_2 (Figure 18 and 19). The model average oxidation state in air for both phases is 2.6-2.7, equivalent to an average valence of 5.2-5.4. This result is roughly consistent with the spectroscopic observations of Fortner *et al.* (1999) which indicated that the uranium in pyrochlore was largely pentavalent. That UO_x is greater than 2.5 indicates that some hexavalent uranium is present; for U^{+4}=0, $UO_{2.6}$ is equivalent to U^{+6}/U^{+5}=0.24.

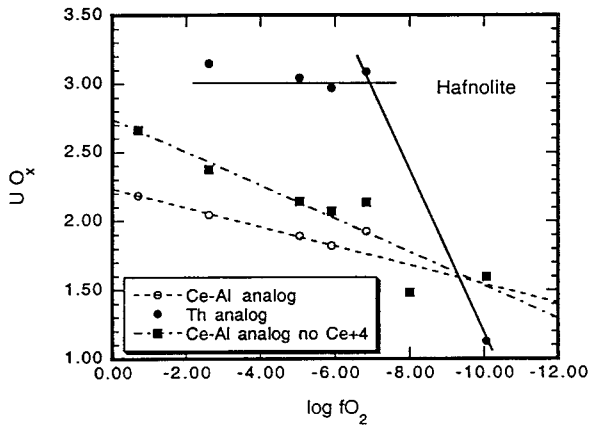

Figure 20. Average uranium oxidation state for hafnolite as a function of log fO_2. The calculation assumes that $Ce^{+4}/\Sigma Ce=0$. UO_x is then adjusted to produce ideal hafnolite stoichiometry (see text).

The hafnolites from the Ce-Al analog are very close to the ideal with the number of oxygens per 4 cations typically greater than 6.9 over the entire range of oxygen fugacities, and greater than 7.0 for the lowest fO_2s (Table 6). If we apply the model described above to these hafnolites, however, we find that the apparent average oxidation state also decreases as a linear function of log fO_2 (Figure 20). Unlike the pyrochlores, UO_x for hafnolite drops below 2 which is, of course, not possible, and indicates that either the oxidation state of cerium must be higher than that prescribed by the model, or that zirconolite is slightly cation deficient. For samples equilibrated at higher fO_2s, the apparent non-stoichiometry can be rectified by reducing all the cerium to Ce^{+3}. However, at lower fO_2s, UO_x required for stoichiometry again falls below the accessible lower bound, UO_2, indicating that hafnolite must be cation deficient at least at the lowest fO_2s, and potentially at higher values. The only other mechanism by which ideal hafnolite stoichiometry can be maintained is by the reduction of Ti^{+4} to Ti^{+3}. In this connection, Begg *et al.* (1998) identified Ti^{+3} in zirconolites synthesized under reducing conditions, and associated the reduction of Ti to the appearance of perovskite in the assemblage. Samples synthesized at the lowest fO_2s in this study do indeed contain perovskite (e.g., samples 7/7, 7/8, 7/9, Table 6). For example, when all the cerium and uranium are cast as +3 and +4, respectively, ideal stoichiometry for sample 7/8 is attained with $Ti^{+3}/\Sigma Ti=0.06$. Given the large number of possible charge-balance mechanisms available, it is clear that direct observational methods are required to fully understand the structural chemistry of these phases.

5.2 Structural components in pyrochlore, brannerite, hafnolite and perovskite

5.2.1 Pyrochlore

Based upon the variations in the stoichiometry and partitioning with changing fO_2 we have inferred progressive changes in the valence and site occupancy of the various

elements investigated. Implicit in this inference is the assumption of a number of endmember components that describe the compositions of the phases in question. In this section we briefly discuss these implicit assignments and the variation in the concentrations of the components chosen with fO_2.

The components chosen to model the composition of pyrochlore should attempt to describe: (1) the increase in U and decrease in Ca and Ce concentrations with decreasing fO_2, (2) the observation that the concentrations of Ca and Ti are always close to 1 and 2 atoms normalized to 4 total cations, respectively, and (3) the inferred reduction of uranium with decreasing fO_2. We have used the following components: $CaUTiAlO_7$, $CaTi_3O_7$, $Ce_2Ti_2O_7$, $Gd_2Ti_2O_7$, $CaHfTi_2O_7$, $CaThTi_2O_7$, $CaUTi_2O_7$, and $Ca_{1.5}U_{0.5}Ti_2O_7$ (Table 7).

Uranium is included in three components, $CaUTi_2O_7$, $CaUTiAlO_7$ and $Ca_{1.5}U_{0.5}Ti_2O_7$ which are neutral species based on the +4, +5 and +6 valence states of uranium and allow the apparent variations in the average oxidation state of uranium inferred above to be accommodated. $Gd_2Ti_2O_7$ and $Ce_2Ti_2O_7$ describe the simple trivalent lanthanide pyrochlores, while $CaHfTi_2O_7$, $CaThTi_2O_7$, $CaUTi_2O_7$ and $CaTi_3O_7$ describe components in which a divalent cation on one of the A-sites is charge-compensated by an equal number of quadravalent cations on the A-site. $CaUTi_2O_7$ assumes that uranium is present as U^{+4}, and $CaTi_3O_7$ allows the number of Ti per 4 cations to exceed 2. Cerium is accommodated only as a trivalent cation in conflict with compositional trends described above and also with direct spectroscopic determinations of cerium valence. Alternative choices of components present other difficulties. For instance, Ce^{+4} could be accommodated in aluminum-bearing components such as $CeAl(AlTi)O_7$ in which charge excess on the A-site is balanced by a deficit on the T-site. However, this restricts the concentration of Ce^{+4} to be no more than half the amount of Al, and Al is a minor component in pyrochlore. Inversions including this component show that its concentration increases with decreasing fO_2 which is counterintuitive. $CaCeTi_2O_7$ is a less restrictive choice, but is related to other components through the reaction,

$$CaCeTi_2O_7 + 1/2\ CaUTi_2O_7 = Ca_{1.5}U_{0.5}Ti_2O_7 + 1/2\ Ce_2Ti_2O_7$$

and yields a singular matrix of inversion.

Through trial and error, we've determined a set of components above yields the fewest number of negative concentrations (Table 7). The major components in the Ce- and Ce/Al analog materials are $Ce_2Ti_2O_7$, $Gd_2Ti_2O_7$, $CaHfTi_2O_7$, $CaUTi_2O_7$, and $Ca_{1.5}U_{0.5}Ti_2O_7$. The concentration of $Gd_2Ti_2O_7$ and $CaHfTi_2O_7$ remain constant with fO_2, while $Ce_2Ti_2O_7$ shows a slight decrease, consistent with the data shown in Figures 3 and 15. As fO_2 decreases the concentration of the quadravalent uranium component, $CaUTi_2O_7$, increases and that of the hexavalent uranium species, $Ca_{1.5}U_{0.5}Ti_2O_7$, decreases (Figure 21). As $Ca_{1.5}U_{0.5}Ti_2O_7$ contains more calcium per formula unit than $CaUTi_2O_7$ this exchange describes the decrease in Ca with fO_2 described in Figures 3 and 15. Similarly, $CaUTiAlO_7$ decreases with fO_2 and $CaTi_3O_7$ increases, consistent with the observed increase in Ti normalized to 4 cations with decreasing fO_2. The compositions of the pyrochlores from each bulk composition are clearly separated on $CaUTi_2O_7$–$Ca_{1.5}U_{0.5}Ti_2O_7$–$CaHfTi_2O_7$ ternary (Figure 21). The concentration of $CaHfTi_2O_7$ is roughly constant for each bulk composition, and the major compositional variation is the exchange of $Ca_{1.5}U_{0.5}Ti_2O_7$ for $CaUTi_2O_7$ as the run conditions become more reducing. At the lowest fO_2s the compositions lie essentially along the $CaHfTi_2O_7$-$CaUTi_2O_7$ join. Qualitatively similar trends are displayed by the Th-bearing materials in which $CaThTi_2O_7$ replaces $Ce_2Ti_2O_7$.

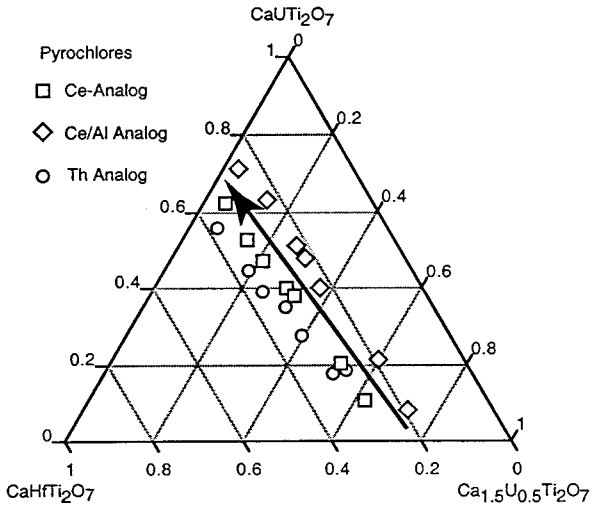

Figure 21. Pyrochlore compositions (mole fractions) in the $CaUTi_2O_7$–$Ca_{1.5}U_{0.5}Ti_2O_7$ –$CaHfTi_2O_7$ ternary.

All the pyrochlores have normalized Ca and Ti concentrations close to 1 and 2, respectively. This is simply a consequence of the fact that the predominant phase in a high-variance phase assemblage reflects the bulk composition of the material, which in this study has a Ca/Ti atom ratio close to 0.5. Unlike zirconolite, there is no structural constraint limiting the amount of Ca on the pyrochlore A-site to 1 Ca normalized to 4 cations. Indeed, Ryerson *et al.* (2000) report pyrochlores coexisting with Ca-perovskites with up to 1.2 Ca normalized to 4 cations.

5.2.2 Brannerite

Brannerite is particularly stable in the Th-analog, occurring over the entire fO_2 range, and the trends in brannerite composition are best illustrated by this composition. An appropriate set of components to describe the compositions of brannerite should help to reconcile the increase in U with fO_2 and the correlated decrease in Ca. We propose the following components: $Ca_{0.5}U_{0.5}Ti_2O_6$, $Ce_{0.5}U_{0.5}Ti_2O_6$, $Gd_{0.5}U_{0.5}Ti_2O_6$, $ThTi_2O_6$, $HfTi_2O_6$, UHf_2O_6, UTi_2O_6 and $UAlTiO_6$ (Table 8). As uranium is the predominant species, it is included in all but 2 of the components. UHf_2O_6 and UTi_2O_6 contain quadravalent uranium, and $Ce_{0.5}U_{0.5}Ti_2O_6$, $Gd_{0.5}U_{0.5}Ti_2O_6$, and $UAlTiO_6$ contain pentavalent uranium. Hexavalent uranium is contained only in $Ca_{0.5}U_{0.5}Ti_2O_6$.

The major compositional variation is expressed in terms of $Ca_{0.5}U_{0.5}Ti_2O_6$, $Gd_{0.5}U_{0.5}Ti_2O_6$ and UTi_2O_6 (Figure 22); $UAlTiO_6$ and UHf_2O_6 are negligible and $ThTi_2O_6$ and $HfTi_2O_6$ are virtually constant. As fO_2 decreases, the concentrations of the hexavalent and pentavalent uranium-bearing species decrease and that of the quadravalent, UTi_2O_6 increases. As $Ca_{0.5}U_{0.5}Ti_2O_6$ is the only Ca-bearing component, its consumption during reduction is consistent with the decreasing Ca normalized to 3 total cations illustrated in Figure 11. Conversely, the increase in the concentration of components with 0.5 uranium per formula unit for UTi_2O_6 with 1 uranium per formula unit explains the increase in U normalized to 3 total cations with decreasing fO_2. The trends for the Ce-Al analog are not as well developed as those for the Th-analog, but are qualitatively consistent.

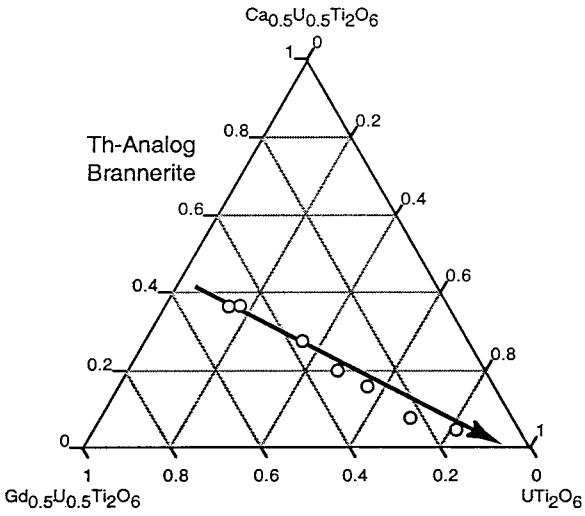

Figure 22. Brannerite compositions (mole fractions) in the $Ca_{0.5}U_{0.5}Ti_2O_6$–$Gd_{0.5}U_{0.5}Ti_2O_6$ UTi_2O_6 ternary.

5.2.3 Hafnolite

Hafnolite, with the structural formula ABT_2O_7, is structurally analogous to zirconolite ($CaZrTi_2O_7$) in which a large radius cation such as a lanthanide is able to occupy the A-site, and is charge compensated by a smaller tri- or divalent cation on the B-site and/or T-site. In this study hafnolite is clearly stabilized by aluminum and is present over the full range of fO_2s for the Ce-Al analog. It is also present in some of the Th-analog materials and in

Table 8. Mole fractions of brannerite components

	$Ca_{0.5}U_{0.5}Ti_2O_6$	$Ce_{0.5}U_{0.5}Ti_2O_6$	$Gd_{0.5}U_{0.5}Ti_2O_6$	$ThTi_2O_6$	$HfTi_2O_6$	UHf_2O_6	UTi_2O_6	$UAlTiO_6$
Ce Analog								
1/4	0.162	0.415	0.271	0.000	0.078	0.018	0.022	0.033
Ce/Al Analog								
7/3	0.167	0.472	0.261	0.000	0.094	*-0.002*	*-0.099*	0.107
7/4	0.142	0.411	0.262	0.000	0.066	0.007	0.037	0.075
7/5	0.089	0.321	0.199	0.000	0.076	0.003	0.257	0.055
Th Analog								
8/3	0.194	0.000	0.258	0.334	0.120	0.012	0.079	0.003
8/4	0.196	0.000	0.247	0.333	0.106	0.010	0.092	0.016
8/5	0.149	0.000	0.202	0.335	0.079	0.020	0.194	0.021
8/6	0.104	0.000	0.169	0.358	0.102	0.008	0.245	0.014
8/9	0.082	0.000	0.145	0.351	0.116	0.006	0.284	0.016
8/7	0.039	0.000	0.113	0.371	0.112	0.007	0.344	0.014
8/8	0.024	0.000	0.069	0.383	0.104	0.010	0.402	0.008

some of the lower fO_2 runs in the Ce-analog. As it doesn't concentrate Th, it is likely that its presence in the Ce- and Th-analog may be related to aluminum impurities from the starting materials or grinding medium.

The discussion here is focussed on the results of the Ce-Al analog runs. At high fO_2s hafnolite, based on Ce^{+3} and U^{+4}, is slightly oxygen deficient, indicating the possibility of higher oxidation states. Using the same basis, hafnolite is slightly cation deficient at low fO_2s, suggestive of Ti^{+3}. The T-site contains less than 2 Ti cations requiring some Al to fill the site completely. There is, however, there is more Al in hafnolite than is required to fill the T-site, indicating that Al is also present on the B-site. A set of components capturing these variations is: $CaHfTi_2O_7$, $CaThTi_2O_7$, $CaUTi_2O_7$, $CaCeTi_2O_7$, $GdUTi_2O_7$, $GdAlTi_2O_7$, $CeAlTi_2O_7$, $Gd(U_{0.5}A_{1.5})AlTiO_7$ (Table 9). The nominal $A^{+2}B^{+4}T^{+4}{}_2O_7$ stoichiometry is expressed by the components $CaCe^{+4}Ti_2O_7$, $CaHfTi_2O_7$, $CaThTi_2O_7$ and $CaUTi_2O_7$. A more complex coupled substitution involving pentavalent uranium is required to form $Gd(U_{0.5}Al_{0.5})(AlTi)O_7$. Here, aluminum resides on both the B- and T-sites. Al on the T-site balances the charge excess produced by placing Gd on the A-site; a coupled substitution of pentavalent uranium and aluminum maintains charge balance on the B-site. Coupled substitution on only the A- and B-sites is required to form the components $GdAlTi_2O_7$ and $Ce^{+3}AlTi_2O_7$ in which the charge excess on the A-site is balanced by Al on the B-site. Finally a reduced component that includes both $U^{+4}$and Ti^{+3} is expressed by $GdUTi_2O_7$; the charge excess on the A-site is balanced by placing Ti^{+3} on the T-site.

When applied to the hafnolites analyzed in the Ce-, Ce/Al- and Th- analog materials, the set of components described above generates a relatively large number of negative concentrations (Table 9a). The absolute value of these negative concentrations is generally less than 0.10, and they are largely observed for the reduced species, $GdUTi_2O_7$, and the component containing quadravalent cerium, $CaCeTi_2O_7$. Otherwise, the major component in each starting composition is $CaHfTi_2O_7$ with subordinate amounts of $CaUTi_2O_7$ and the aluminum-bearing components. The concentration of the pentavalent uranium-bearing species, $Gd(U_{0.5}Al_{0.5})(AlTi)O_7$, decreases with decreasing fO_2 and is balanced by a correlated increase in the quadravalent uranium-bearing species $CaUTi_2O_7$.

Due to the complicated formulation of the hafnolite components, positive concentrations of Ce-bearing components are generated for the Th-analog even though it contains no cerium (Table 9a). An alternative set of components not including cerium-bearing species is a more suitable choice for this composition. To complete the matrix (7 cations X 7 components) we add $Ca(Gd_{0.5}U_{0.5})Ti_2O_7$, which involves a coupled substitution of 0.5 Gd + 0.5 U $\leftrightarrow$ Ca the B-site. This alternative set of components decreases the number of negative concentrations (Table 9b), and yields qualitatively similar trends to the

Table 9. Mole fractions of hafnolite components in Th-analog								
	$CaHfTi_2O_7$	$CaThTi_2O_7$	$CaUTi_2O_7$	$CaCeTi_2O_7$	$GdUTi_2O_7$	$GdAlTi_2O_7$	$CeAlTi_2O_7$	$Gd(U_{0.5}Al_{0.5})AlTiO_7$
Ce-Al analog								
7/3	0.616	0.000	0.098	0.062	*-0.043*	0.017	0.050	0.201
7/4	0.634	0.000	0.090	0.021	*-0.016*	0.039	0.075	0.157
7/5	0.673	0.000	0.072	*-0.031*	*-0.004*	0.037	0.124	0.129
7/6	0.601	0.000	0.124	*-0.046*	*-0.035*	0.146	0.149	0.060
7/9	0.538	0.000	0.188	*-0.087*	*-0.096*	0.221	0.193	0.045
7/7	0.575	0.000	0.158	*-0.104*	*-0.044*	0.165	0.211	0.039
7/8	0.534	0.000	0.192	*-0.136*	*-0.023*	0.225	0.234	-0.026
Ce analog								
1/9	0.752	0.000	0.030	*-0.015*	0.039	0.071	0.102	0.021
1/7	0.769	0.000	0.021	*-0.027*	0.053	0.071	0.111	0.004
1/8	0.729	0.000	0.046	*-0.043*	0.079	0.137	0.127	-0.076
Th analog								
8/4	0.792	0.018	0.082	0.080	*-0.045*	0.088	*-0.080*	0.066
8/5	0.778	0.023	0.093	0.062	*-0.052*	0.102	*-0.062*	0.056
8/6	0.835	0.022	0.040	0.044	*-0.027*	0.033	*-0.044*	0.097
8/9	0.792	0.026	0.069	0.043	*-0.050*	0.075	*-0.043*	0.088
8/8	0.724	0.045	0.101	*-0.085*	0.019	0.188	0.085	*-0.077*

Table Xb. Concentrations of alternate hafnolite components in Th-analog							
	$CaHfTi_2O_7$	$CaThTi_2O_7$	$CaUTi_2O_7$	$GdUTi_2O_7$	$GdAlTi_2O_7$	$CaGd_{.05}U_{0.5}Ti_2O_7$	$Gd(U_{0.5}Al_{0.5})AlTiO_7$
8/4	0.792	0.018	0.002	*-0.045*	0.008	0.160	0.066
8/5	0.778	0.023	0.030	*-0.052*	0.040	0.125	0.056
8/6	0.835	0.022	*-0.004*	*-0.027*	*-0.011*	0.088	0.097
8/9	0.792	0.026	0.025	*-0.050*	0.031	0.087	0.088
8/8	0.724	0.045	0.186	0.019	0.272	*-0.169*	*-0.077*

original component set in which U^{+5} components are consumed during reduction, replaced by U^{+4}-bearing components.

5.3.4 Perovskite

Perovskite, nominally $CaTiO_3$, is cation deficient in these experiments and commonly has ~1 Ti cation per 2 total cations (Tables 4 and 6). A charge excess is produced on the Ca-site if the remaining cations are assigned there, suggesting that all of the vacancies reside on the Ca-site. With the exception of $CeAlO_2$, in which Ce^{+3} on the Ca-site is compensated by Al on the Ti-site, we have chosen components that have either 1 Ti or 1 Hf per 2 cations. The non-stoichiometry is assigned to the Ca-site alone resulting in the following components: $CaTiO_3$, $CaHfO_2$, $\square_{0.33}Al_{0.66}TiO_3$, $\square_{0.33}Ce_{0.66}TiO_3$, $\square_{0.33}Gd_{0.66}TiO_3$, $CeAlO_2$, $\square_{0.5}Th_{0.5}TiO_3$, $\square_{0.5}U_{0.5}TiO_3$ (where $\square$ is a cation vacancy). The only stoichiometric components are $CaTiO_3$, $CaHfO_3$, and $CeAlO_2$. The others all have vacancies on the Ca-site. Negative concentrations are obtained are for only $\square_{0.33}Al_{0.66}TiO_3$ and even these are not significantly different from zero (Table 10). $CaTiO_3$ and $\square_{0.33}Ce_{0.66}TiO_3$ are the predominant species with minor $\square_{0.33}Gd_{0.66}TiO_3$.

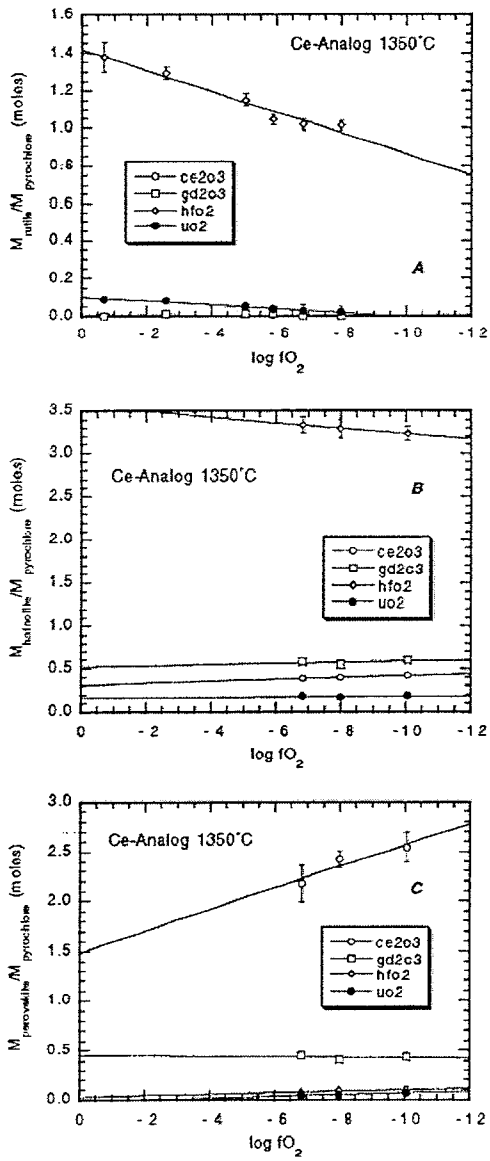

Figure 23. Partition coefficients as a function of oxygen fugacity for the Ce-analog experiments. (A) rutile/pyrochlore, (B) hafnolite/pyrochlore, (C) perovskite/pyrochlore.

5.3 Element Partitioning

The smooth variation in mineral composition with changing fO_2 is reflected in similar variations in the partition coefficients which are qualitatively similar for each of the analog compositions (Figures 23, 23, 24). All of the partition coefficients are given relative to pyrochlore and expressed as oxide molar

ratios.

The data are sparse for the Ce-analog due to the low number of phases found in the runs performed at higher fO_2s. The greatest number of data are for rutile-pyrochlore partitioning and demonstrate the relative incompatibility of uranium in rutile relative to pyrochlore ($D^{rut/py} < 0.1$). The incompatibility becomes more pronounced with decreasing fO_2 (Fig. 23a). This variation with fO_2 is also the case for hafnium which favors rutile at

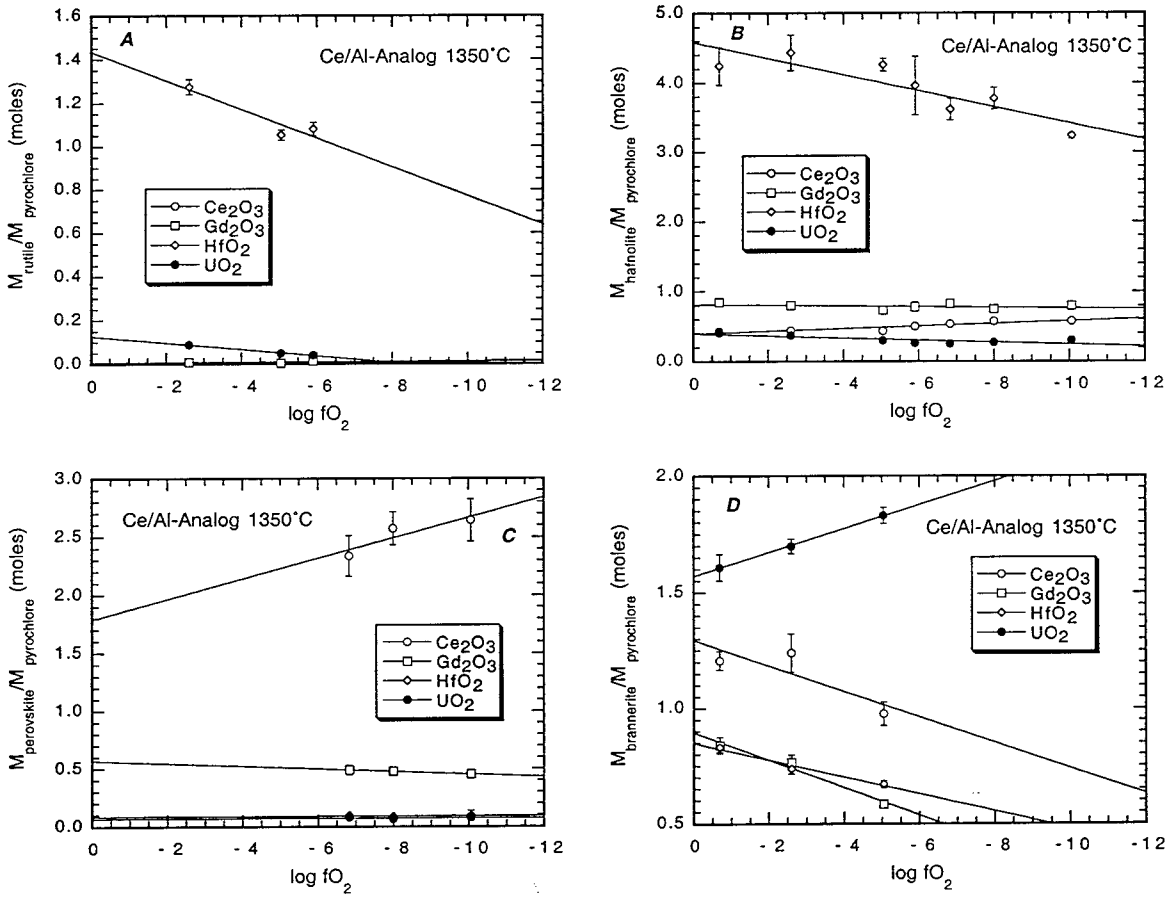

Figure 24. Partition coefficients as a function of oxygen fugacity for the Ce-analog experiments. (A) rutile/pyrochlore, (B) hafnolite/pyrochlore, (C) perovskite/pyrochlore, (D) brannerite/pyrochlore.

high fO_2, and is equally partitioned between rutile and pyrochlore ($D^{rut/py}$ = 1.0) at –log fO_2= 10 (Fig. 23a). Hafnium is strongly partitioned into hafnolite relative to pyrochlore (Figure 23b). The composition of hafnolite is also relatively constant in these experiments which is demonstrated by the constant values of $D^{hfn/py}$ for Ce_2O_3, Gd_2O_3, HfO_2 and UO_2 (Figure 23b). The lanthanides are fractionated by pyrochlore and perovskite, with Ce compatible in perovskite and Gd more compatible in pyrochlore (Fig. 23c). $D^{pv/py}$ for

Table 10. Mole fractions of perovskite components

	$\square_{0.33}Al_{0.66}TiO_3$	$CaTiO_3$	$\square_{0.33}Ce_{0.66}TiO_3$	$\square_{0.33}Gd_{0.66}TiO_3$	$CeAlO_2$	$\square_{0.5}Th_{0.5}TiO_3$	$\square_{0.5}U_{0.5}TiO_3$	$CaHfO_2$
Ce Analog								
1/7	0.001	0.612	0.335	0.071	0.024	0.000	0.021	0.010
1/8	-0.006	0.610	0.331	0.075	0.023	0.000	0.030	0.010
1/9	0.004	0.620	0.323	0.074	0.023	0.000	0.019	0.008
Ce/Al Analog								
7/7	0.002	0.621	0.265	0.076	0.064	0.000	0.030	0.006
7/8	-0.002	0.638	0.236	0.076	0.067	0.000	0.040	0.008
7/9	0.000	0.629	0.250	0.076	0.065	0.000	0.035	0.007

Gd_2O_3 is constant with respect to changing fO_2, but that of Ce increases with decreasing fO_2 (Figure 23c). The changing behavior of Ce relative to Gd may indicate that at least some cerium is present in the quadravalent state, and becomes more compatible in perovskite as it is converted to Ce^{+3}. However, the pyrochlore structure is capable of accommodating a wide variety of composition variations, and the partitioning of cerium could be changing in response to changes in other components.

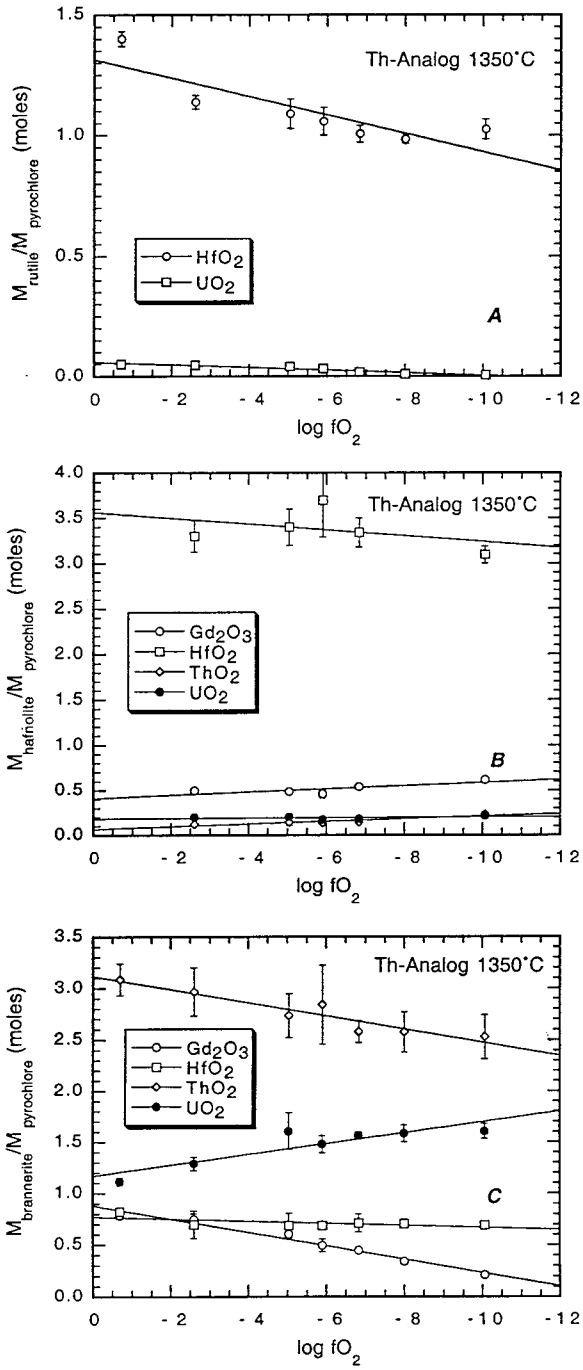

Figure 25. Partition coefficients as a function of oxygen fugacity for the Th-analog experiments. (A) rutile/pyrochlore, (B) hafnolite/pyrochlore, (C) brannerite/pyrochlore.

The major effect of adding Al_2O_3 to the Ce-analog is to stabilize hafnolite over the full range of fO_2s sampled. In addition, brannerite is also stable in a greater number of runs and an Al-rich accessory phase is always present. However, the addition of Al_2O_3 has little effect on the values of the partition coefficients relative to those in the Al-free Ce-analog. For instance, the values of $D^{rut/py}$ are virtually indistinquishable in these two compositions (Figure 23a and 24a). Similarly, the values of $D^{hfn/py}$ for are quite similar in both relative and absolute magnitude in both compositions (Figure 23b and 24b), though a slight decrease in $D^{hfn/py}$ for cerium is suggested by the greater number of data for the Ce/Al analog. $D^{pv/py}$ for the Ce-Al analog is also virtually identical to that in the Al-free

composition and confirms that fractionation of Ce and Gd by these phases (Figure 23c). The negligible effect of aluminum on the partitioning relationships is consistent with the partitioning of aluminum itself which is strongly concentrated in Al-rich accessory minerals. The low concentrations in hafnolite, pyrochlore, rutile and perovskite preclude any coupled substitutions based on Al-rich components that would affect changes in the activity-composition relationships for the other elements.

Brannerite in also stable is some of the higher fO_2 runs from the Ce-Al analog. The broad range in pyrochlore compositions observed in the CaO-HfO_2-UO_2 ternary (Figure 14) is reflected in variations of $D^{brn/py}$ with fO_2 (Fig 24d). Consistent with the increased U concentrations with fO_2 (Figure 18), $D^{brn/py}$ for UO_2 increases as fO_2 falls (Figure 24d). $D^{brn/py}$ for Ce, Gd and Hf display the opposite effect. The increase in $D^{brn/py}$ with fO_2 may reflect the reduction of uranium shown in Figure 19.

Unlike uranium, thorium does not enter rutile in detectable amounts (Table 7). It does, however, enter pyrochlore (~8 wt%) and hafnolite (~1 wt%). Nevertheless, the effect on the partitioning of other elements (Gd, U and Hf) between pyrochlore, hafnolite and rutile is negligible (Figure 25a, b). This is consistent with Th forming a $CaThTi_2O_7$ component in both pyrochlore and hafnolite, which dilutes that other components, but doesn't alter their activity-composition relationships.

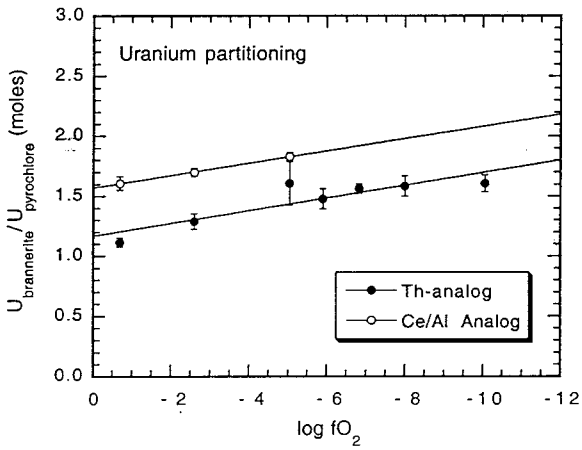

Figure 26. Partitioning of uranium between brannerite and pyrochlore for the Th and Ce/Al analogs.

The major effect of thorium addition is the stabilization of brannerite under all conditions (Table 3). $D^{brn/py}$ is between 2.5 and 3 over the range of fO_2s sampled, and its enrichment in brannerite stabilizes that phase. While $D^{brn/py}$ for thorium decreases slightly with decreasing fO_2, $D^{brn/py}$ for uranium increases (Figure 25c) which may reflect the conversion of U^{+6} to U^{+4}. However, even at the lowest fO_2s, where our model calculations indicate that virtually all of the uranium is present at U^{+4} (Figure 18 and 19), $D^{brn/py}$ for Th is greater that $D^{brn/py}$ for uranium indicating that Th^{+4} is more compatible in brannerite than U^{+4} (Fig. 25c). This conclusion is consistent with the observation that $D^{brn/py}$ for uranium in the Ce/Al analog samples is always higher than it is in the Th-analog at the same fO_2(Figure 26).

Thorium and cerium were both intended to act a analogs for plutonium, and the variation of $D^{brn/py}$ with fO_2 for these element (as well as gadolinium) is similar (Figure 25). However, the absolute value of $D^{brn/py}$ is quite different, however, as thorium is more than a factor of two more strongly enriched in brannerite than cerium. $D^{brn/py}$ for cerium more closely resembles that of gadolinium, suggesting that cerium is trivalent in these experiments (Fig. 27).

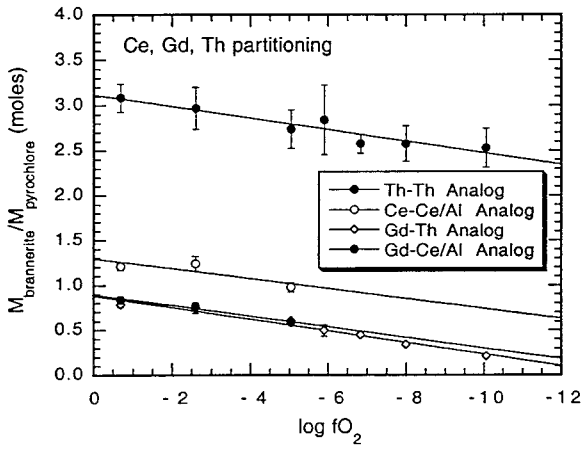

Figure 27. Partitioning of Ce, Gd and Th between brannerite and pyrochlore for the Th and Ce/Al analogs.

5.4 Phase equilibria

The compositions and synthesis conditions used in these experiments result in high variance phase assemblages in which the number of chemical components exceeds the number of phases. As such, the compositions of the phases are constrained largely by the bulk composition of the starting material rather than by phase equilibria. Taken to its extreme, in an assemblage with only one phase that phase has the exact composition of the starting material. Here the system is characterized by 8 components: Al, Ca, Ti, ±Ce, Gd, Hf, ±Th, U and O_2, when cast as elements. The greatest number of phases produced is 5 in some of the Ce/Al analog runs, resulting in a variance of 4 under fixed pressure conditions. Nevertheless, we can use the information from some of the lower variance assemblages in the Th-analog and Ce/Al analog experiments to observe how the compositions of coexisting phases vary with fO_2.

The compositions of rutile, hafnolite and the calcium aluminotitanate phase are relatively constant in these experiments compared with those of pyrochlore and brannerite. As such, they can be used as "projection points' from which the compositions of phases with these minerals can be projected from n-dimensional compositional space into the ternary systems of interest. By constraining the assemblages to be in equilibrium with these saturating phases, we buffer the activities of these components described by the projection points, eliminating the effect of variations in these activities on the compositions of the coexisting minerals. In all cases, these are simplifications as the number of phases present is not sufficient to buffer all of the components within the system.

In the Th-analog runs all of the experiments are saturated in rutile and hafnolite. We have projected the compositions of coexisting pyrochlore and brannerite onto the UO_2'-

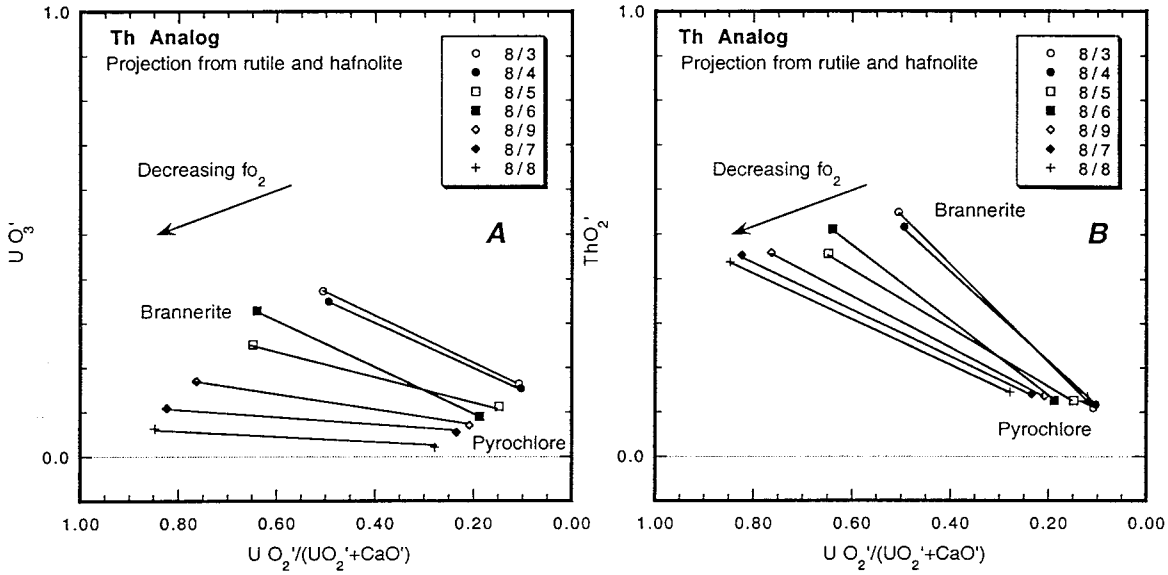

Figure 28. "Phase diagram" for the Th-analog experiments. (A) Projection from rutile and hafnolite onto the UO_2'=CaO'-UO_3' plane – "prime" indicates that these are projection components which are not equivalent to the real, measured components. The valence state of uranium is calculated assuming ideal trivalent cerium. (B) Projection from rutile and hafnolite onto the UO_2'-CaO'-ThO_2 plane.

CaO'-ThO_2' and UO_2'-CaO'-UO_3' ternaries in Figure 28. The "prime" indicates that these are the projected components resulting from the transformation of coordinates and not the measured chemical concentrations. Orthogonal projections are used to facilitate the plotting of negative components. The concentrations of UO_2 and UO_3 were calculated using the ideal model oxygen stoichiometry in Table 7.

The position and variation with fO_2 of brannerite-pyrochlore tielines is similar in both the UO_2'-CaO'-ThO_2' and UO_2'-CaO'-UO_3' projections. The high fO_2 runs plot on the low UO_2'/(UO_2'+CaO') side of the diagram and move progressively to higher values as fO_2 decreases. In general, the tielines do not cross indicating that the bulk UO_2'/(UO_2'+CaO') is increasing as uranium is reduced from U^{+6} to U^{+4}. This is clearly shown in the UO_3' concentrations of the coexisting phases in the UO_2'-CaO'-UO_3' projection (Figure 28a). The changing slope of the brannerite-pyrochlore tieline on the UO_2'-CaO'-UO_3' projection indicates that the brannerite-pyrochlore partition coefficient for U^{+6} decreases with fO_2. However, the bulk partition coefficient for UO_2 (all U^{+4}) increases with decreasing fO_2 (Fig 25c) indicating that the increase in $D^{brn/py}$ for quadravalent U more than compensates for the decrease in U^{+6}. The brannerite-pyrochlore tielines on the UO_2'-

CaO'-ThO_2' projection are much closer to parallel that those in the UO_2'-CaO'-UO_3 projection, and the variation in the ThO_2' concentration is much less pronounced. This is consistent with the single valence state for Th.

Rutile and hafnolite can also be used to project the compositions of coexisting phases in the Ce/Al analog into various ternary systems. The position of the 3-phase assemblage, brannerite-pyrochlore-calcium aluminotitanate, projected on the UO_2'-CaO'-UO_3' shows the variation in uranium oxidation state with changing fO_2 (Figure 29a); U^{+6} is calculated assuming all of the cerium is present as Ce^{+3} and stoichiometry is ideal. At high fO_2 the three phase field lies at low $UO_2'/(UO_2'+CaO')$. As fO_2 is reduced, the field rotates counterclockwise as uranium is reduced. As in the Th-analog, the brannerite-pyrochlore

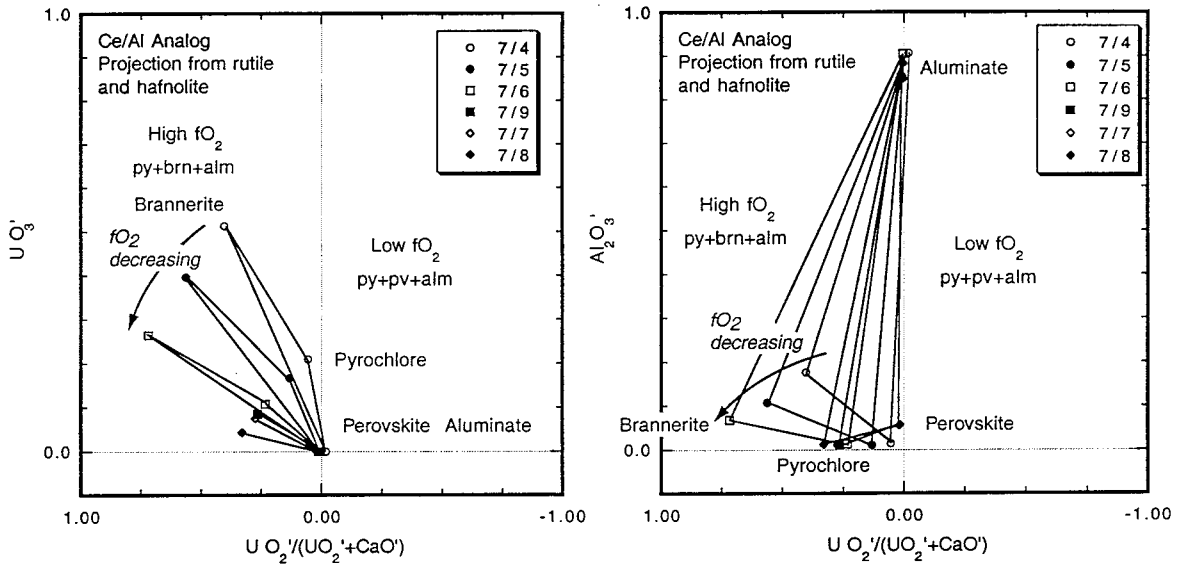

Figure 29. "Phase diagram" for the Ce/Al-analog experiments. (A) Projection from rutile and hafnolite onto the UO_2'=CaO'-UO_3' plane – "prime" indicates that these are projection components which are not equivalent to the real, measured components. The valence state of uranium is calculated assuming ideal trivalent cerium. (B) Projection from rutile and hafnolite onto the UO_2'-CaO'-Al_2O_3' plane.

partition coefficient for uranium decreases with decreasing fO_2. As the field rotates the pyrochlore approaches colinearity with brannerite and the aluminotitanate and brannerite disappears and is replaced by perovskite.

Perovskite and the calcium aluminotitanate phase plot at the same point in the UO_2'-CaO'-UO_3' projection, obscuring the phase relationships. They are better observed on the UO_2'-CaO'-Al_2O_3' projection (Figure 29b). At high fO_2 the assemblage is pyrochlore, brannerite, aluminate, rutile and hafnolite. As fO_2 decreases brannerite becomes depleted

in Al_2O_3' and the pyrochlore-brannerite tieline rotates toward the x-axis. Eventually brannerite becomes unstable and is replaced by perovskite. Pyrochlore continues to increase in UO_2' as it is now the only significant host for uranium. The reaction sequence in this projection has crossing tielines largely due to its inability of represent the uranium reduction that occurs.

6. Conclusions

Ce-, Th- and Al-doped Ce-analogs of titanate-based Pu-immobilization ceramics demonstrate systematic variations in mineral chemistry and phase assemblage with variations in oxygen fugacity. These variations seem to be largely due to the reduction of uranium under more reducing conditions. In spite variations in fO_2 of greater than 10 orders of magnitude, all of the phases encountered here have been previously observed in the SYNROC family of titanate ceramics (Ringwood et al., 1979; Ryerson, 1984; Lumpkin et al., 1994); Ryerson (1984) obtained similar results for a SYNROC formulation for the immobilization of US Defense wastes. The desired phase assemblage, pyrochlore+brannerite+rutile is favored by more oxidizing conditions, however. Reduction leads to the formation of perovskite and a calcium aluminotitanate. Both of these phases incorporate lanthanides in the analog materials, and are likely to incorporate plutonium in the actual immobilization wasteform.

References

Armstrong, J.T. CITZAF: a package of correction programs for the quantitative electron microbeam analysis of thick polished materials, thin films and particles. *Microbeam Anal.*, **4**, 177-200, 1995.

Ebbinghaus, B.B., C. Cicero-Herman, L. Gray and H. Shaw, Plutonium immobilization project: Baseline Formulation, Lawrence Livermore National Laboratory, 1999.

Lumpkin, G.R., K.P. Hart, P.J. McGlinn, and T.E. Payne, Retention of actinides in natural pyrochlores and zirconolites, *Radiochimica Acta*, **66/67**, 460-474, 1994.

Ringwood, A.E., S.E. Kesson, N.G. Ware, W. Hibberson, and A. Major, Immobilization of high level nuclear reactor waste in SYNROC, *Nature*, **278**, 219-223, 1979.

Ryerson, F.J., Phase equilibria in nuclear waste ceramics: The effect of oxygen fugacity, *J. Am. Ceram. Soc*, **67**, 75-82, 1984.

Subramanian, M.A., G. Aravamudan, and G.V. Subba Rao, Oxide pyrochlores-A review, *Progress in Solid State Chemistry*, **15**, 55-143, 1983.

Appendix A. Electron Probe Standards and x-ray lines

Element	X-Ray Lines	Standard
Al	$Al_{K\alpha}$	Al_2O_3
Ca	$Ca_{K\alpha}$	$CaSiO_3$
Ti	$Ti_{K\alpha}$	TiO_2
Ce	$Ce_{L\beta 1}$	CeO_2
Gd	$Gd_{L\beta 1}$	Gadolinium Gallium Garnet
Hf	Hf_L	Hf-Zr alloy
Th	$Th_{M\beta 1}$	ThO_2
U	$U_{M\beta 1}$	UO_2